J. Fluid Mech. (2006), *vol.* 555, *pp.* 149–176.
doi:10.1017/S0022112006008846 Printed in the United Kingdom

Euler-alpha and vortex blob regularization of vortex filament and vortex sheet motion

By D. D. HOLM[1,2], M. NITSCHE[3] AND V. PUTKARADZE[4]

[1]Computational and Computer Science Division, MS D413, Los Alamos National Laboratory, Los Alamos, NM 87545, USA

[2]Department of Mathematics, Imperial College London, London SW7 2AZ, UK

[3]Department of Mathematics and Statistics, University of New Mexico, Albuquerque, NM 87131, USA

[4]Department of Mathematics, Colorado State University, Fort Collins, CO 80523, USA

(Received 29 June 2005 and in revised form 28 October 2005)

The Euler-alpha and the vortex blob model are two different regularizations of incompressible ideal fluid flow. Here, a regularization is a smoothing operation which controls the fluid velocity in a stronger norm than L^2. The Euler-alpha model is the inviscid version of the Lagrangian averaged Navier–Stokes-alpha turbulence model. The vortex blob model was introduced to regularize vortex flows. This paper presents both models within one general framework, and compares the results when applied to planar and axisymmetric vortex filaments and sheets. By certain measures, the Euler-alpha model is closer to the unregularized flow than the vortex blob model. The differences that result in circular vortex filament motion, vortex sheet linear stability properties, and core dynamics of spiral vortex sheet roll-up are discussed.

1. Introduction

This paper presents a numerical comparison of weak vorticity solutions for two regularizations of the Euler equations, namely the Lagrangian averaged Euler-alpha model and the vortex blob model. The work is motivated by the computation of vortex sheet motion. A vortex sheet is an inviscid model for a shear layer which approximates the layer by a surface. The vorticity is a delta function on the surface and the tangential velocity component is discontinuous across it. The governing Euler equations reduce to an integro-differential equation for the evolution of the vortex sheet position, thus reducing the problem dimension by one. However, a numerical discretization by the point vortex approximation breaks down after a finite time. It has been established that even with analytic initial data, the sheet develops a singularity in finite time in which its curvature blows up (Moore 1979; Meiron, Baker & Orszag 1982; Krasny 1986*a*; Shelley 1992; Caflisch *et al.* 1993; Cowley, Baker, & Tanveer 1999). The point vortex approximation converges before this critical time (Caflisch, Hou & Lowengrub 1999), but no longer converges at later times (Krasny 1986*a*). The approach taken to compute the motion past singularity formation is to regularize the flow by introducing a numerical smoothing parameter into the governing equations. The vortex sheet is defined as the limit of zero smoothing parameter, that is, a limit of a sequence of approximate solutions. For a discussion of the theory of these approximate-solution sequences, see Majda & Bertozzi (2002).

The regularizations considered are typically inviscid. We note that in a physical problem, the regularizing mechanism is by fluid viscosity and the limit of interest

is that of vanishing viscosity. However, solving the full viscous problem for small viscosity is highly computationally expensive. The vortex sheet model and its inviscid regularizations are of intrinsic mathematical interest, but also provide a computationally more feasible approach. Comparisons between inviscid regularizations and real fluid flows (Nitsche & Krasny 1994) as well as solutions to the full viscous problem (Tryggvason, Dahm & Sbeih 1991) indicate good agreement at large scales. An important open question is whether the limiting behaviour depends on the regularization, be it viscous or not. This paper compares two inviscid regularizations.

The most common vortex sheet regularization is the vortex blob model, in which the singular Biot-Savart kernel is replaced by a convolution with an algebraically decaying smooth function, and the vortex sheet evolution is computed in a Lagrangian framework moving with the fluid particles. The algebraically decaying smoothing operator, introduced by Rosenhead (1930), was first applied to planar vortex sheets (Chorin & Bernard 1973; Anderson 1985; Krasny 1986*b*) and has since been extended to axisymmetric and three-dimensional flows (see the reviews by Leonard 1985; Puckett 1993; Meiburg 1995; Cottet & Koumoutsakos 2000). Alternative regularizations proposed by Beale & Majda (1985) (see also Cottet & Koumoutsakos 2000) use smoothing functions with different decay properties in the far field, and were recently applied to vortex sheets by Baker & Pham (2005). Other kinds of regularizations have also been proposed. Baker & Shelley (1990) studied constant vorticity layers in the limit of vanishing thickness and Hou, Lowengrub & Shelley (1997) proposed surface tension as the regularizing mechanism.

The Euler-alpha model was first introduced in the Euler–Poincaré variational framework by Holm, Marsden & Ratiu (1998*a*, *b*) as a generalization of the Camassa–Holm shallow-water equation (Camassa & Holm 1993) to the case of n-dimensional incompressible flow. It may also be found by applying Lagrangian averaging to the Euler equations and introducing a closure assumption based on Taylor's hypothesis that small rapid fluctuations are swept along with the flow. Chen *et al.* (1999) introduced viscosity into the Euler-alpha equation and compared its steady solutions with experimental data for the mean velocity of turbulence in pipes and channels. The close agreement of this comparison ignited a series of investigations of these equations as a new type of turbulence model. The Euler-alpha model preserves the Lie–Poisson Hamiltonian structure of the Euler equations and satisfies a circulation theorem, so that circulation of filaments is preserved. The Euler-alpha regularization of vortex filaments is discussed in Holm (2003). Other special features and theoretical results are reviewed in Holm *et al.* (1998*a*, *b*) and Shkoller (2000). The Euler-alpha model is usually implemented in an Eulerian framework, and has never before been applied to compute vortex sheet motion.

Foias, Holm & Titi (2001) show that the Euler-alpha averaging process replaces the transport velocity by a smoothed velocity obtained by convolution, similar to the vortex blob case. However, the Euler-alpha regularization stands out: unlike any regularization previously applied to vortex sheets, the Euler-alpha smoothing function is unbounded at the origin and is in this sense closer to the unregularized flow. The natural question that arises is whether and how this affects the vortex sheet evolution. This is the motivation for the present work. We apply the Euler-alpha regularization to vortex sheets and compare with known vortex blob results. We also obtain results for the velocity of regularized circular filaments.

A connection between the Euler-alpha and the vortex blob model has previously been explored by Oliver & Shkoller (2001), who study the Euler-alpha equations in a Lagrangian framework. They show that for smooth vorticity distributions, the

solutions converge as the regularization parameter vanishes. Our paper concerns weak solutions for singular vorticity distributions, such as filaments and sheets. We remark that throughout, we denote by *Euler-alpha* the regularization and associated convolution operator introduced by Holm *et al.* (1998*a*, *b*) and by *vortex blob* the convolution operator used by Chorin & Bernard (1973). This differs from the language of Oliver & Shkoller (2001), who use vortex blob to denote that, in contrast to previous formulations of the Euler-alpha model, their scheme is Lagrangian and not Eulerian.

The paper is organized as follows. Section 2 presents the general framework which describes both the Euler-alpha and the vortex blob regularization. Section 3 presents the specific smoothing operators in each case, and addresses regularized straight and circular vortex filaments. Section 4 concerns the linear stability properties of the regularized vortex sheet. Section 5 compares the regularized vortex sheet motion for a model problem, both in planar and axisymmetric geometry. The main results are summarized in § 6. The Appendix presents an analytical approximation of the self-induced velocity of an axisymmetric filament, regularized by Euler-alpha.

2. The general framework

The following framework is given in Foias *et al.* (2001). Let $\boldsymbol{v}$ be an incompressible velocity field. In all the examples in this paper, $\boldsymbol{v}$ is the singular velocity induced by a vortex filament or a vortex sheet, and therefore is referred to as the *singular velocity*. Define

$$\boldsymbol{u} = L(\boldsymbol{v}) = h \star \boldsymbol{v}, \tag{2.1}$$

where h is in the Sobolev space H^1. Then $\boldsymbol{u}$ is smoother than $\boldsymbol{v}$ and is referred to as the *regularized velocity*. Define the *singular vorticity* $\boldsymbol{q}$ and the *regularized vorticity* $\boldsymbol{\omega}$ by

$$\boldsymbol{q} = \nabla \times \boldsymbol{v} \quad \text{and} \quad \boldsymbol{\omega} = \nabla \times \boldsymbol{u}.$$

Since $h \in H^1$, the convolution operator L commutes with differentiation and therefore $\nabla \cdot \boldsymbol{u} = 0$ and $\boldsymbol{\omega} = L(\boldsymbol{q})$. The Euler-alpha and the vortex blob models are two examples corresponding to different functions h, which will be given below.

Using Hamilton's principle, the pair $(\boldsymbol{u}, \boldsymbol{v})$ can be shown to satisfy the Euler–Poincaré equation,

$$\partial_t \boldsymbol{v} - \boldsymbol{u} \times (\nabla \times \boldsymbol{v}) - \nabla \Pi = 0, \tag{2.2}$$

where Π is a generalized pressure term. The system (2.2) preserves the Hamiltonian structure of the Euler equations. The equations of motion can be derived from the Hamiltonian $H(\boldsymbol{x})$, which is conserved in time. It is given by

$$H = \tfrac{1}{2} \int \psi(\boldsymbol{x}) \cdot \boldsymbol{q}(\boldsymbol{x}) \, \mathrm{d}\boldsymbol{x} = \tfrac{1}{2} \int \boldsymbol{u}(\boldsymbol{x}) \cdot \boldsymbol{v}(\boldsymbol{x}) \, \mathrm{d}\boldsymbol{x}, \tag{2.3}$$

where ψ is the streamfunction associated with the regularized velocity $\boldsymbol{u}$, $\Delta \psi = -\nabla \times \boldsymbol{u}$. The form of the Hamiltonian therefore depends on the particular regularizing function h. Furthermore, if h is invariant under translation and rotation, as is the case for the Euler-alpha and the vortex blob regularizations, the linear and angular momenta,

$$L(t) = \tfrac{1}{2} \int \boldsymbol{q} \times \boldsymbol{x} \, \mathrm{d}\boldsymbol{x} = \int \boldsymbol{v} \, \mathrm{d}\boldsymbol{x}$$

and

$$I(t) = -\tfrac{1}{2} \int |\boldsymbol{x}|^2 \boldsymbol{q} \, \mathrm{d}\boldsymbol{x} = \int \boldsymbol{v} \times \boldsymbol{x} \, \mathrm{d}\boldsymbol{x},$$

are also conserved, as outlined in Appendix A.

Taking the curl of (2.2), we obtain the equivalent evolution equation

$$\partial_t \boldsymbol{q} + \boldsymbol{u} \cdot \nabla \boldsymbol{q} - \boldsymbol{q} \cdot \nabla \boldsymbol{u} = 0, \tag{2.4}$$

which states that the singular vorticity is convected and stretched by the regularized velocity. Note that (2.4) implies the circulation theorem

$$\frac{\mathrm{d}}{\mathrm{d}t} \oint_{c(\boldsymbol{u})} \boldsymbol{v} \cdot \mathrm{d}\boldsymbol{x} = 0, \tag{2.5}$$

where the loop $c(\boldsymbol{u})$ moves with the regularized velocity and the integrand contains the singular velocity. Conversely, Foias *et al.* (2001) showed that Hamilton's equations can be derived from the circulation theorem. The existence of a circulation theorem distinguishes the Euler-alpha model from large-eddy simulation models for turbulence such as the Leray model, which do not satisfy a circulation theorem in the inviscid limit. Since filament circulation is conserved, so is the fluid helicity, given by the Casimir function, $C(t) = \int \boldsymbol{v} \cdot \boldsymbol{q} \, \mathrm{d}\boldsymbol{x}$. Any regularization (2.1) for which h is invariant under translation and rotation therefore satisfies the same Hamiltonian properties and conservation laws as the Euler equations (see Appendix A).

If, in addition, L is invertible, the regularized vorticity satisfies the partial differential equation

$$\partial_t \boldsymbol{\omega} + L(\boldsymbol{u} \cdot \nabla \boldsymbol{q}) - L(\boldsymbol{q} \cdot \nabla \boldsymbol{u}) = 0, \tag{2.6}$$

provided $\boldsymbol{q} = L^{-1}(\boldsymbol{\omega})$ is sufficiently smooth. For a large class of operators of interest, it is easy to show that L^{-1} exists in the proper functional space, as follows. Consider functions $h(\boldsymbol{x})$ which depend on $r = |\boldsymbol{x}|$ only. In that case, the operator L is self-adjoint in the Hilbert space $\mathscr{L}_2$. If we further assume that $h(r) > 0$ and all components of $\boldsymbol{q}$ are non-negative, as is the case in all our examples, then $L^* \boldsymbol{q} = 0$ means $\boldsymbol{q} = 0$ almost everywhere, so $\mathrm{Ker} L^* = 0$ and the inverse operator exists. Equation (2.6) solves for $\boldsymbol{\omega} = L\boldsymbol{q}$. In order to obtain $\boldsymbol{u} = L\boldsymbol{v}$, it is necessary for L to commute with curl^{-1}. This is true since for incompressible fields $\boldsymbol{q}$ on $\Re^3$, $curl^{-1} = curl(1/\Delta)$, and L commutes both with curl and with the integral operator $1/\Delta$.

The regularization (2.1) is obtained by specifying the operator L (that is, the function h) or L^{-1}, if it exists. Alternatively, we can specify a function G such that

$$\boldsymbol{u} = \nabla \times (G \star \boldsymbol{q}). \tag{2.7}$$

The relation between G and h is obtained as follows. Let $\psi = G \star \boldsymbol{q}$. Since $\boldsymbol{u} = \nabla \times \psi$, $-\nabla \times \boldsymbol{u} = \Delta \psi$ and therefore $\psi = -\Delta^{-1} \nabla \times L(\boldsymbol{v}) = -\Delta^{-1} L(\boldsymbol{q})$. That is,

$$G \star \boldsymbol{q} = -\Delta^{-1} L(\boldsymbol{q}) \tag{2.8}$$

and therefore

$$L(\boldsymbol{q}) = -\Delta G \star \boldsymbol{q} = h \star \boldsymbol{q}. \tag{2.9}$$

It follows that

$$h = -\Delta G.$$

The next section specifies the smoothing operator for the two specific regularizations considered in this paper.

3. Euler-alpha and vortex blob model

3.1. *Three-dimensional flow*

3.1.1. *The Euler-alpha model*

The Euler-alpha model refers to the case given by the Helmholtz operator,

$$L^{-1} = 1 - \alpha^2 \Delta, \tag{3.1}$$

where $\alpha > 0$ is a numerical parameter. The limit $\alpha \to 0$ corresponds to the unregularized case $\boldsymbol{u} = \boldsymbol{v}$. The functions h_α and G_α corresponding to this operator in three dimensions depend on $r = |\boldsymbol{x}|$ only, and are given by

$$h_\alpha(r) = \frac{\mathrm{e}^{-r/\alpha}}{4\pi\alpha^2 r}, \tag{3.2}$$

$$G_\alpha(r) = \frac{1 - \mathrm{e}^{-r/\alpha}}{4\pi r}. \tag{3.3}$$

Equation (3.2) follows from the fact that h_α is the fundamental solution of the Helmholtz operator, $L^{-1}h_\alpha = (1 - \alpha^2\Delta)h_\alpha = \delta_{3d}$, where δ_{3d} is the delta-function in three dimensions, and therefore

$$L^{-1}(h_\alpha \star \boldsymbol{v}) = \boldsymbol{v} \Rightarrow L(\boldsymbol{v}) = h_\alpha \star \boldsymbol{v}. \tag{3.4}$$

To confirm (3.3), note that $G_\alpha = g - \alpha^2 h_\alpha$ where $g = 1/4\pi r$ is the fundamental solution of the negative Laplacian, $\Delta g = -\delta$, and thus

$$\begin{aligned} L^{-1}(-\Delta)G_\alpha &= -\Delta L^{-1} G_\alpha = -\Delta(1 - \alpha^2\Delta)(g - \alpha^2 h_\alpha) \\ &= -\Delta g + \alpha^2 \Delta(\Delta g) + \alpha^2 \Delta(1 - \alpha^2 \Delta) h_\alpha \\ &= \delta_{3d} - \alpha^2 \Delta\delta + \alpha^2 \Delta \delta_{3d} = \delta_{3d}. \end{aligned} \tag{3.5}$$

Alternatively, we can confirm that $h_\alpha = -\Delta G_\alpha$.

The corresponding regularized velocity induced by a singular vorticity $\boldsymbol{q}$ is obtained from the relation

$$\begin{aligned} \boldsymbol{u}_\alpha(\boldsymbol{x}) &= \nabla \times (G_\alpha \star \boldsymbol{q}) = \nabla_x \times \int G_\alpha(|\boldsymbol{x} - \boldsymbol{y}|)\boldsymbol{q}(\boldsymbol{y})\,\mathrm{d}\boldsymbol{y} \\ &= \int \nabla_x \times [G_\alpha(\rho)\boldsymbol{q}(\boldsymbol{y})]\,\mathrm{d}\boldsymbol{y} = \int \nabla_x [G_\alpha(\rho)] \times \boldsymbol{q}(\boldsymbol{y})\,\mathrm{d}\boldsymbol{y} \\ &= \int G'_\alpha(\rho)\nabla_x \rho \times \boldsymbol{q}(\boldsymbol{y})\,\mathrm{d}\boldsymbol{y} = \int G'_\alpha(\rho)\frac{\boldsymbol{x} - \boldsymbol{y}}{\rho} \times \boldsymbol{q}(\boldsymbol{y})\,\mathrm{d}\boldsymbol{y} \\ &= -\frac{1}{4\pi}\int \frac{1 - \mathrm{e}^{-\rho/\alpha}(1 + \rho/\alpha)}{\rho^3}(\boldsymbol{x} - \boldsymbol{y}) \times \boldsymbol{q}(\boldsymbol{y})\,\mathrm{d}\boldsymbol{y}, \end{aligned} \tag{3.6}$$

where $\rho = |\boldsymbol{x} - \boldsymbol{y}|$.

3.1.2. *The vortex blob model*

The vortex blob model consists of regularizing the fluid velocity by convolution, as in (2.1). It is implemented by transporting vortex filaments with the regularized velocity while keeping the circulation constant, which solves (2.4) in a Lagrangian framework. Vortex blob solutions thus fit in the same general framework as the Euler-alpha model, albeit with a different smoothing operator. The regularization commonly used is that introduced by Rosenhead (1930), given by

$$G_\delta(r) = \frac{1}{4\pi\sqrt{r^2 + \delta^2}}, \tag{3.7}$$

with corresponding function

$$h_\delta(r) = -\Delta G = \frac{3\delta^2}{4\pi(r^2+\delta^2)^{5/2}} \tag{3.8}$$

and induced velocity

$$\begin{aligned} \boldsymbol{u}_\delta(\boldsymbol{x}) = \nabla \times (G_\delta \star \boldsymbol{q}) &= \int G'_\delta(\rho)\frac{\boldsymbol{x}-\boldsymbol{y}}{\rho} \times \boldsymbol{q}(\boldsymbol{y})\,\mathrm{d}\boldsymbol{y} \\ &= -\frac{1}{4\pi}\int \frac{1}{(\rho^2+\delta^2)^{3/2}}(\boldsymbol{x}-\boldsymbol{y}) \times \boldsymbol{q}(\boldsymbol{y})\,\mathrm{d}\boldsymbol{y}. \end{aligned} \tag{3.9}$$

Throughout this paper, this vortex blob regularization is denoted by subscript δ, while subscripts α denote the classical Euler-alpha regularization. Notice that in the vortex blob case, the operator L^{-1} is not stated explicitely. For non-negative components of the vorticity $\boldsymbol{q}$, it is known to exist from our earlier remarks, but it does not have a finite differential operator representation as in the Euler-alpha case.

3.1.3. *Behaviour near the origin*

Alternative vortex blob kernels such as the one proposed by Beale & Majda (1985)

$$h_\sigma(r) = \frac{\mathrm{e}^{-r^3/\sigma^3}}{4\pi\sigma^2} \tag{3.10}$$

have also been used (see Cottet & Koumoutsakos 2000; Baker & Pham 2005). While those kernels have different decay behaviour from the Rosenhead kernel for large r (h_σ is exponentially decaying while h_δ is algebraically decaying), they have similar behaviour near the origin: all the standard vortex blob regularizations are bounded at the origin.

The Euler-alpha regularization on the other hand presents a new feature. The kernel h_α is unbounded at the origin, and is, in this sense, closer to the unregularized case, in which $h = \delta$. This makes a comparison with the vortex blob regularization particularly interesting. The decay of the Euler-alpha kernel as $r \to \infty$ is exponential.

3.2. *Planar flow*

3.2.1. *The Euler-alpha model*

The functions G and h corresponding to $L^{-1} = 1 - \alpha^2\Delta$ in two dimensions are found using the fundamental solutions $g = (1/2\pi)\log r$ and $h = (1/2\pi\alpha^2)K_0(r/\alpha)$ of the Laplace and the Helmholtz operator, respectively, where K_ν is the modified Bessel function of the second kind and $r = \sqrt{x^2+y^2}$. (To confirm that h solves $L^{-1}h = (1-\alpha^2\Delta)h = \delta_{2d}$, where δ_{2d} is the delta-function in two dimensions, use Bessel's equation $r^2K_0''(r) + rK_0'(r) - r^2K_0(r) = 0$ to show $L^{-1}h = 0$ for $r \neq 0$, and use the two properties $K_0(r) \sim -\log r$ as $r \to 0$, $K_0(r) \sim 1/r$ as $r \to \infty$ to show $\int_{\Re^2} L^{-1}h = 1$.) Using the same arguments as in § 3.1, it follows that in two dimensions

$$h_\alpha(r) = \frac{1}{2\pi\alpha^2}K_0\left(\frac{r}{\alpha}\right), \tag{3.11}$$

$$G_\alpha(r) = -(g + \alpha^2 h) = -\frac{1}{2\pi}\left[\log r + K_o\left(\frac{r}{\alpha}\right)\right], \tag{3.12}$$

Using Bessel's equation, we can check that $h = -\Delta G$. Note that as in three dimensions, G_α is bounded for $\alpha > 0$, but h_α is not.

For the purpose of this paper, we require the corresponding velocity $(u, v)(x, y; x_o, y_o)$ at (x, y) induced by a point vortex of strength Γ_o at (x_o, y_o) with vorticity

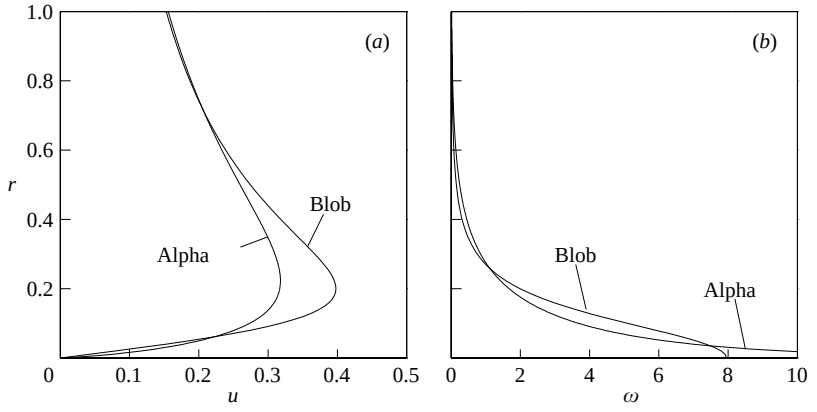

FIGURE 1. (*a*) Azimuthal velocity and (*b*) scalar vorticity induced by a regularized point vortex of unit circulation $\boldsymbol{q} = \delta_{2d}\boldsymbol{k}$ at distance r from the vortex. Results using the Euler-alpha and the vortex blob model with $\alpha = \delta = 0.2$ are shown, as indicated.

$\boldsymbol{q} = \Gamma_o \delta_{2d}(x - x_o, y - y_o)\boldsymbol{k}$, where $\boldsymbol{k}$ is the unit vector in the z-direction. From $\boldsymbol{u} = u\boldsymbol{i} + v\boldsymbol{j} = \nabla \times \psi = \nabla \times (G \star \boldsymbol{q})$, and using that $K_o'(r) = -K_1(r)$, it follows that

$$u_\alpha(x, y; x_o, y_o) = \Gamma_o \frac{\partial G_\alpha}{\partial y} = -\frac{\Gamma_o}{2\pi}\frac{y - y_o}{\rho^2}\left[1 - \frac{\rho}{\alpha}K_1\left(\frac{\rho}{\alpha}\right)\right], \tag{3.13a}$$

$$v_\alpha(x, y; x_o, y_o) = -\Gamma_o \frac{\partial G_\alpha}{\partial x} = \frac{\Gamma_o}{2\pi}\frac{x - x_o}{\rho^2}\left[1 - \frac{\rho}{\alpha}K_1\left(\frac{\rho}{\alpha}\right)\right], \tag{3.13b}$$

where $\rho = |\boldsymbol{x} - \boldsymbol{y}| = \sqrt{(x - x_o)^2 + (y - y_o)^2}$. Notice that the regularized velocity is bounded at the origin since $K_1(r) \sim 1/r$ as $r \to 0$, but the regularized vorticity $\omega_\alpha(x, y; x_o, y_o) = -\Gamma_o \Delta G_\alpha = \Gamma_o h_\alpha(\rho)$ is not.

3.2.2. *The vortex blob model*

The functions G and h corresponding to the vortex blob regularization in planar two-dimensional flow are

$$G_\delta(r) = -\frac{1}{4\pi}\log(r^2 + \delta^2), \tag{3.14}$$

$$h_\delta(r) = \frac{\delta^2}{\pi(r^2 + \delta^2)^2}. \tag{3.15}$$

The corresponding velocity induced by a point vortex $\boldsymbol{q} = \Gamma_o \delta_{2d}(x - x_o, y - y_o)\boldsymbol{k}$ is

$$u_\delta(x, y; x_o, y_o) = -\frac{\Gamma_o}{2\pi}\frac{y - y_o}{r^2 + \delta^2}, \tag{3.16a}$$

$$v_\delta(x, y; x_o, y_o) = \frac{\Gamma_o}{2\pi}\frac{x - x_o}{r^2 + \delta^2}, \tag{3.16b}$$

with vorticity $\omega_\delta(x, y; x_o, y_o) = \Gamma_o h_\delta(\rho)$.

3.2.3. *Comparison for point vortex*

Figure 1 shows the radial velocity and vorticity distributions for a planar point vortex of unit strength, regularized by the Euler-alpha and the vortex blob model as indicated, with $\alpha = \delta = 0.2$. Here, r is plotted in the vertical direction, and u, ω on the horizontal. Notice that for $\alpha = \delta$, the maximum velocity is smaller in the Euler-alpha

case, but the velocity hugs the axis more closely, owing to its more singular nature. The corresponding vorticity is unbounded at the origin in the Euler-alpha case, but bounded in the blob case, as discussed earlier. The difference between exponential and algebraic decay as $r \to \infty$ is not visible at this scale. For $r > 1$, it is visible in the vorticity, but not in the velocity. Both velocities decay as $1/r$.

3.3. *Axisymmetric flow*

3.3.1. *The Euler-alpha model*

Axisymmetric flow is described in cylindrical coordinates (x, y, θ), where x is the axis of symmetry, $y \geqslant 0$ is the radial coordinate, and θ is the azimuthal coordinate. In no-swirl axisymmetric flow, the vorticity points in the azimuthal direction and the vortex filaments are circles centred on the axis. For a single vortex filament of strength Γ_o at $(x, y) = (x_o, y_o)$, the vorticity is a delta-function on the filament,

$$\boldsymbol{q} = \Gamma_o \delta_{2d}(x - x_o, y - y_o)\boldsymbol{e}_\theta, \tag{3.17}$$

where $\boldsymbol{e}_\theta = -\sin\theta\, \boldsymbol{e}_y + \cos\theta\, \boldsymbol{e}_z$ is the unit vector in the azimuthal direction, and $\boldsymbol{e}_x, \boldsymbol{e}_y, \boldsymbol{e}_z$ are unit vectors in the x-, y- and z- directions.

The velocity induced by the circular filament at a point $\boldsymbol{x}$ in the symmetry plane is obtained from (3.6). Let $\boldsymbol{x} = x\boldsymbol{e}_x + y\boldsymbol{e}_y$ be a point in the symmetry plane, and $\boldsymbol{y} = x_o\boldsymbol{e}_x + y_o\cos\theta\, \boldsymbol{e}_y + y_o \sin\theta\, \boldsymbol{e}_z$ be a point on the vortex filament. Then

$$\rho = |\boldsymbol{x} - \boldsymbol{y}| = \sqrt{(x - x_o)^2 + y^2 + y_o^2 - 2yy_o\cos\theta} \tag{3.18}$$

and

$$(\boldsymbol{x} - \boldsymbol{y}) \times \boldsymbol{e}_\theta = (y\cos\theta - y_o)\boldsymbol{e}_x - \cos\theta(x - x_o)\boldsymbol{e}_y - \sin\theta(x - x_o)\boldsymbol{e}_z.$$

It follows by symmetry, that the velocity component in the z-direction is zero (i.e. the azimuthal velocity is zero). The velocity components (u, v) in the x- and y-directions are given by

$$u_\alpha(x, y; x_o, y_o) = -\frac{\Gamma_o}{4\pi}\int_0^{2\pi} \frac{1 - \mathrm{e}^{-\rho/\alpha}(1 + \rho/\alpha)}{\rho^3}(y\cos\theta - y_o)\, y_o\, \mathrm{d}\theta, \tag{3.19a}$$

$$v_\alpha(x, y; x_o, y_o) = \frac{\Gamma_o}{4\pi}\int_0^{2\pi} \frac{1 - \mathrm{e}^{-\rho/\alpha}(1 + \rho/\alpha)}{\rho^3}(x - x_o)\cos\theta y_o\, \mathrm{d}\theta, \tag{3.19b}$$

Details on how these are computed numerically will be given in § 5.4.1. The corresponding azimuthal vorticity component $\omega_\alpha = \partial v_\alpha/\partial x - \partial u_\alpha/\partial y$ is most easily obtained by computing $\boldsymbol{\omega} = h_\alpha \star \boldsymbol{q}$, with h as in (3.2) and $\boldsymbol{q}$ as in (3.17). It is

$$\omega_\alpha(x, y; x_o, y_o) = \frac{\Gamma_o}{4\pi\alpha^2}\int_0^{2\pi} \frac{\mathrm{e}^{-\rho/\alpha}}{\rho}\cos\theta\, y_o\, \mathrm{d}\theta. \tag{3.20}$$

3.3.2. *The vortex blob model*

It follows from (3.9) and (3.17) that the velocity induced at (x, y) by a vortex filament of strength Γ_o positioned at $(x, y) = (x_o, y_o)$ is

$$u_\delta(x, y; x_o, y_o) = -\frac{\Gamma_o}{4\pi}\int_0^{2\pi} \frac{y\cos\theta - y_o}{(\rho^2 + \delta^2)^{3/2}}\, y_o\, \mathrm{d}\theta, \tag{3.21a}$$

$$v_\delta(x, y; x_o, y_o) = \frac{\Gamma_o}{4\pi}\int_0^{2\pi} \frac{(x - x_o)\cos\theta}{(\rho^2 + \delta^2)^{3/2}}\, y_o\, \mathrm{d}\theta, \tag{3.21b}$$

where ρ is as in (3.18). The integrals in (3.21) can be expressed in terms of elliptic integrals which can be efficiently evaluated. The corresponding azimuthal vorticity

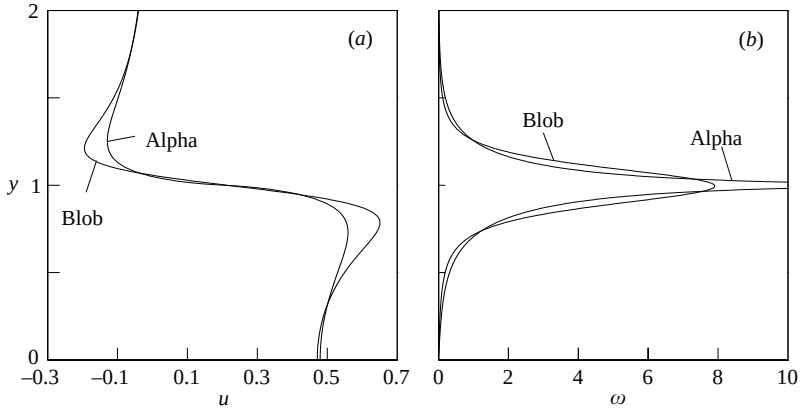

FIGURE 2. (*a*) Radial velocity and (*b*) azimuthal vorticity induced by a regularized vortex ring of unit radius and circulation along a vertical line through the vorticity maximum. Results using the vortex blob and the Euler-alpha model with $\alpha = \delta = 0.2$. are shown, as indicated.

component $\omega_\delta = v_x - u_y$ is again computed using $\boldsymbol{\omega} = h_\delta \star \boldsymbol{q}$ with h_δ as in (3.8) and $\boldsymbol{q}$ as in (3.17). It is

$$\omega_\delta(x, y; x_o, y_o) = \frac{3\Gamma_o y_o \delta^2}{4\pi} \int_0^{2\pi} \frac{\cos\theta}{(\rho^2 + \delta^2)^{5/2}}\, \mathrm{d}\theta. \tag{3.22}$$

Alternatively, ω_δ can be written in terms of elliptic integrals by differentiating the corresponding expressions for u_δ, v_δ.

3.3.3. *Comparison for axisymmetric vortex filament*

Figure 2 compares the regularized velocity and vorticity on a vertical line $x = x_0$ through a vortex ring of unit radius, $y_0 = 1$, and unit circulation. The maximal absolute velocities in the vortex blob case are slightly larger, as in the planar case. At the ring, the Euler-alpha vorticity is unbounded, whereas it is bounded and smooth in the vortex blob case. Note that in the Euler-alpha case, the vorticity (3.20) can be expanded in terms of elliptic integrals that blow up logarithmically as $(x, y) \to (x_o, y_o)$.

3.3.4. *Self-induced velocity*

Consider a circular vortex filament of strength Γ at $x = x_o$ with radius $y_o = R$. In the Appendix, we show that the self-induced velocity under Euler-alpha regularization is

$$\begin{aligned} u_\alpha(x_o, R) &= \frac{\Gamma}{4\pi R}\left[Ein\left(\frac{2R}{\alpha}\right) - 1 + \ln(2) - \frac{3\alpha^2}{8R^2} + O\left(\frac{\alpha^4}{R^4}\right)\right] \\ &\approx \frac{\Gamma}{4\pi R}\left[\ln\left(\frac{R}{\alpha}\right) - 1 + 2\ln(2) + 0.577220 - \frac{3\alpha^2}{8R^2} + error + O\left(\frac{\alpha^4}{R^4}\right)\right], \end{aligned} \tag{3.23}$$

where $error < 0.5 \times 10^{-5}$, assuming that $2R/\alpha > 10$.

We can compare this result to the self-induced velocity of a ring of radius R, circulation Γ, and coresize ϵ given by (Saffman 1992, § 10.2),

$$u_\epsilon(x_0, R) = \frac{\Gamma}{4\pi R}\left(\log\frac{8R}{\epsilon} - \frac{1}{4}\right)\left[1 + O\left(\frac{\epsilon^2}{R^2}\log\frac{R}{\epsilon}\right)\right]. \tag{3.24}$$

It follows that a circular filament regularized by Euler-alpha has, to first order, the same velocity as a ring of finite coresize

$$\epsilon \approx 2.4\alpha. \tag{3.25}$$

A circular filament of radius $y_0 = R$, regularized by the vortex blob model, can be shown to have self-induced velocity

$$u_\delta(x_0, R) = \frac{1}{4\pi R}\left[\log\frac{8R}{\delta} - 1 + O\left(\frac{\delta^2}{R^2}\right)\right]. \tag{3.26}$$

Comparing with (3.24) shows this to be roughly the same as the velocity of a ring of coresize

$$\epsilon \approx 2.1\delta. \tag{3.27}$$

Thus, for equal parameter $\alpha = \delta$, the vortex blob model gives a slightly faster self-induced velocity than the Euler-alpha model.

4. Vortex sheet motion

4.1. *Evolution equations*

A vortex sheet in either planar or axisymmetric flow is defined by a curve $(x(\xi, t), y(\xi, t))$ in a cross-section of the fluid domain, chosen to be the (x, y)-plane, and by its circulation $\Gamma(\xi)$. As before, in the axisymmetric case, x denotes the axis of symmetry, and y is the radial coordinate. The curve is parameterized with respect to a Lagrangian variable $\xi \in I \subset \Re$ that remains constant along fluid particles. The circulation $\Gamma(\xi)$ is the total circulation between $(x(\xi, t), y(\xi, t))$ and a particular particle on the sheet, $(x(\xi_o, t), y(\xi_o, t))$. In the absence of interfacial forces such as surface tension, the circulation is Lagrangian as well, $\mathrm{d}\Gamma/\mathrm{d}t = 0$. The sheet may therefore also be parameterized by Γ.

The vortex sheet is a superposition of point vortices in the planar case, and circular vortex filaments in the axisymmetric case. The governing Euler equations are therefore

$$\frac{\mathrm{d}x}{\mathrm{d}t} = \int_I u(x, y; \widetilde{x}, \widetilde{y})\,\mathrm{d}\widetilde{\Gamma}, \quad \frac{\mathrm{d}y}{\mathrm{d}t} = \int_I v(x, y; \widetilde{x}, \widetilde{y})\,\mathrm{d}\widetilde{\Gamma}, \tag{4.1}$$

where $x = x(\Gamma, t)$, $y = y(\Gamma, t)$, $\widetilde{x} = x(\widetilde{\Gamma}, t)$, $\widetilde{y} = y(\widetilde{\Gamma}, t)$ and $u(x, y, ; \widetilde{x}, \widetilde{y})$, $v(x, y, ; \widetilde{x}, \widetilde{y})$ are the horizontal and vertical velocities at x, y induced by a point vortex and an axisymmetric filament at $(\widetilde{x}, \widetilde{y})$, respectively.

The sheet is subject to the Kelvin–Helmholtz instability. Small perturbations of a flat sheet, with wavenumber k, grow exponentially fast with magnitude e^{wt} with dispersion relation

$$w(k) = k/2. \tag{4.2}$$

As a result, even with analytic initial data, solutions to (4.1) develop singularities in finite time, and past this time, numerical discretizations no longer converge. To compute vortex sheet motion past singularity formation, the fluid velocity is regularized in such a way that the growth rate of the high wavenumber modes is damped, $w_\delta(k) \to 0$ as $k \to \infty$.

Here, we regularize the motion by replacing u, v in (4.1) by the Euler-alpha and vortex blob velocities (3.13), (3.16) and (3.19), (3.21) in the planar and axisymmetric case, respectively. Before presenting solutions to the full equations, the next section compares the dispersion relation obtained with the two regularizations.

4.2. *Linear stability analysis*

4.2.1. *Euler-α regularization*

The flat vortex sheet $x(\Gamma, t) = \Gamma$, $y(\Gamma, t) = 0$ is an equilibrium solution of the governing equations. Linear stability results are obtained by considering the evolution of small perturbations under a linear approximation of the governing equations about the equilibrium. For the Euler-alpha regularization, the governing equations are

$$x_t = -\frac{1}{2\pi}\int_{-\infty}^{\infty} \frac{y-\widetilde{y}}{\rho^2}\left[1-\frac{\rho}{\alpha}K_1\left(\frac{\rho}{\alpha}\right)\right]\mathrm{d}\widetilde{\Gamma}. \tag{4.3a}$$

$$y_t = \frac{1}{2\pi}\int_{-\infty}^{\infty} \frac{x-\widetilde{x}}{\rho^2}\left[1-\frac{\rho}{\alpha}K_1\left(\frac{\rho}{\alpha}\right)\right]\mathrm{d}\widetilde{\Gamma}, \tag{4.3b}$$

where $\rho^2 = (x-\widetilde{x})^2 + (y-\widetilde{y})^2$, $x = x(\Gamma, t)$, $\widetilde{x} = x(\widetilde{\Gamma}, t)$, etc. Consider a small perturbation of the flat sheet

$$x(\Gamma, t) = \Gamma + p(\Gamma, t), \quad y(\Gamma, t) = q(\Gamma, t). \tag{4.4}$$

Substitute into (4.3) and expand the integrands, keeping only linear terms in p, q, to obtain the linear equations for the perturbation p, q:

$$p_t = -\frac{1}{2\pi}\int_{-\infty}^{\infty} \frac{q-\tilde{q}}{(\Gamma-\widetilde{\Gamma})^2}\left[1-\frac{|\Gamma-\widetilde{\Gamma}|}{\alpha}K_1\left(\frac{|\Gamma-\widetilde{\Gamma}|}{\alpha}\right)\right]\mathrm{d}\widetilde{\Gamma}, \tag{4.5a}$$

$$q_t = -\frac{1}{2\pi}\int_{-\infty}^{\infty}(p-\tilde{p})\left[\frac{1-(|\Gamma-\widetilde{\Gamma}|/\alpha)K_1(|\Gamma-\widetilde{\Gamma}|/\alpha)}{(\Gamma-\widetilde{\Gamma})^2} - \frac{K_o(|\Gamma-\widetilde{\Gamma}|/\alpha)}{\alpha^2}\right]\mathrm{d}\widetilde{\Gamma}. \tag{4.5b}$$

Look for solutions of the form $p = P\mathrm{e}^{wt}\mathrm{e}^{\mathrm{i}k\Gamma}$, $q = Q\mathrm{e}^{wt}\mathrm{e}^{\mathrm{i}k\Gamma}$. Substitute into (4.5) to obtain

$$Pw = -\frac{Q}{2\pi}\int_{-\infty}^{\infty}\frac{1-\mathrm{e}^{\mathrm{i}ku}}{u^2}\left[1-\frac{|u|}{\alpha}K_1\left(\frac{|u|}{\alpha}\right)\right]\mathrm{d}u, \tag{4.6a}$$

$$Qw = -\frac{P}{2\pi}\int_{-\infty}^{\infty}\frac{1-\mathrm{e}^{\mathrm{i}ku}}{u^2}\left[1-\frac{|u|}{\alpha}K_1\left(\frac{|u|}{\alpha}\right)\right] - (1-\mathrm{e}^{\mathrm{i}ku})K_o\left(\frac{|u|}{\alpha^2}\right)\mathrm{d}u. \tag{4.6b}$$

This system can be written as

$$Pw = -\frac{Q}{\alpha}I_1(\alpha k), \quad Qw = -\frac{P}{\alpha}I_2(\alpha k), \tag{4.7}$$

where

$$I_1(k) = \frac{1}{\pi}\int_0^{\infty}\frac{1-uK_1(u)}{u^2}(1-\cos ku)\,\mathrm{d}u, \tag{4.8a}$$

$$I_2(k) = I_1 - \frac{1}{\pi}\int_0^{\infty}K_o(u)(1-\cos ku)\,\mathrm{d}u. \tag{4.8b}$$

The system has a non-trivial solution if the dispersion relation,

$$w^2 = \frac{1}{\alpha^2}I_1(\alpha k)I_2(\alpha k), \tag{4.9}$$

is satisfied. Thus, for each wavenumber there is a growing and a decaying mode with growth rate $w(k) = \pm\sqrt{I_1 I_2}/\alpha$. Next, we reproduce these arguments for the vortex blob method.

4.2.2. *Vortex blob regularization*

In this case, the governing equations are

$$x_t = -\frac{1}{2\pi}\int_{-\infty}^{\infty} \frac{y-\widetilde{y}}{r^2+\delta^2}\,\mathrm{d}\widetilde{\Gamma}, \tag{4.10a}$$

$$y_t = \frac{1}{2\pi}\int_{-\infty}^{\infty} \frac{x-\widetilde{x}}{r^2+\delta^2}\,\mathrm{d}\widetilde{\Gamma}. \tag{4.10b}$$

Following the same steps as before, obtain the linear system for P and Q,

$$Pw = -\frac{Q}{\alpha} I_3(\alpha k), \quad Qw = -\frac{P}{\alpha} I_4(\alpha k), \tag{4.11}$$

where

$$I_3(k) = \frac{1}{2\pi}\int_{-\infty}^{\infty} \frac{1-\mathrm{e}^{\mathrm{i}ku}}{u^2+1}\,\mathrm{d}u, \tag{4.12a}$$

$$I_4(k) = I_3 - \frac{1}{\pi}\int_{-\infty}^{\infty} \frac{1-\mathrm{e}^{\mathrm{i}ku}}{(u^2+1)^2}\,\mathrm{d}u. \tag{4.12b}$$

These integrals can be evaluated using the residue theorem to obtain the dispersion relation

$$w^2 = \frac{k\mathrm{e}^{-k\delta}(1-\mathrm{e}^{-k\delta})}{4\delta}. \tag{4.13}$$

Krasny (1986*a*) derived the dispersion relation in the vortex blob case using the periodic kernel and obtained the dispersion relation

$$\widetilde{w}^2 = \frac{\tilde{k}\exp(-\tilde{k}\cosh^{-1}(1+\tilde{\delta}^2))(1-\exp(-\tilde{k}\cosh^{-1}(1+\tilde{\delta}^2)))}{4\tilde{\delta}\sqrt{2+\tilde{\delta}^2}}. \tag{4.14}$$

The relations (4.13) and (4.14) agree in the limit as $\delta \to 0$, with $\widetilde{w} = w/(2\pi)$, $\tilde{k} = k/(2\pi)$ and $\tilde{\delta} = \sqrt{2}\pi\delta$. That is, with this change of variables, the following holds

$$\lim_{\delta\to 0}\max_{k}(\tilde{w}(k) - w(k)) = 0. \tag{4.15}$$

The difference between (4.13) and (4.14) stems from differences between the regularization of the infinite kernel used here and the regularization of the periodic kernel used by Krasny.

4.2.3. *Comparison of dispersion relations*

Figure 3 plots the dispersion relations $w(k)$ for the Euler-alpha regularization (solid curves) and for the vortex blob regularization (dashed curves), for three values of $\alpha = \delta = 0.4, 0.2, 0.1$, as indicated. The dispersion in the unregularized case, $w = k/2$, is also shown (dotted line). Here, the integrals I_1, I_2 are evaluated numerically.

In both regularizations, the growth rates of the low modes approach the unregularized case as $k \to 0$, while the high modes are damped. In the vortex blob case, it is evident from (4.13) that $w(k) \to 0$ as $k \to \infty$, exponentially fast.

In the Euler-alpha model, the high modes appear to decay slower. To determine the decay rate, we investigate the limiting behaviour of I_1 and I_2 as $k \to \infty$ numerically. The integrals (4.8) are computed using the trapezoid rule on a finite domain $[0, b]$, with n points, and b and n are increased until the results have converged to 10 digits in both parameters. The results are shown in figure 4. Figures 4(*a*) and 4(*b*) plot I_1 and $\mathrm{d}I_1/\mathrm{d}k$ *vs.* k, and indicate that $I_1 \to 1/2$ as $k \to \infty$. Figure 4(*c*) plots $\log I_2$ *vs.*

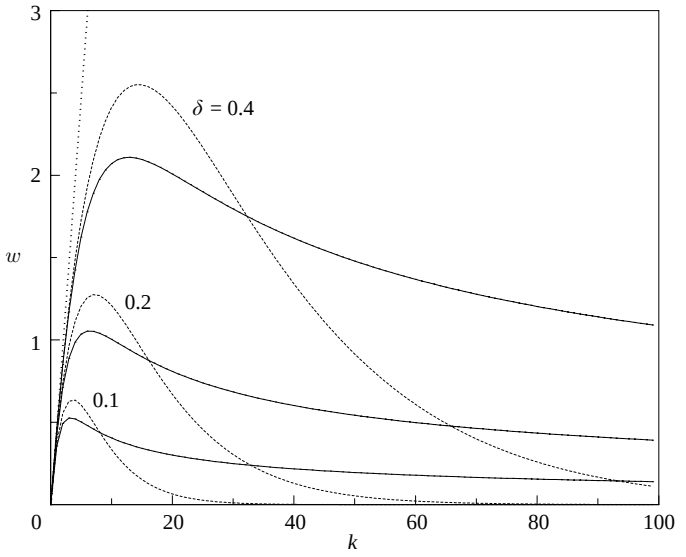

FIGURE 3. Linear growth rates w *vs.* k of a perturbation of a flat vortex sheet, for the Euler-alpha regularization (solid) and the vortex blob regularization (dashed), with the indicated values of the parameter $\alpha = \delta$. The dotted curve shows the result in the unregularized case.

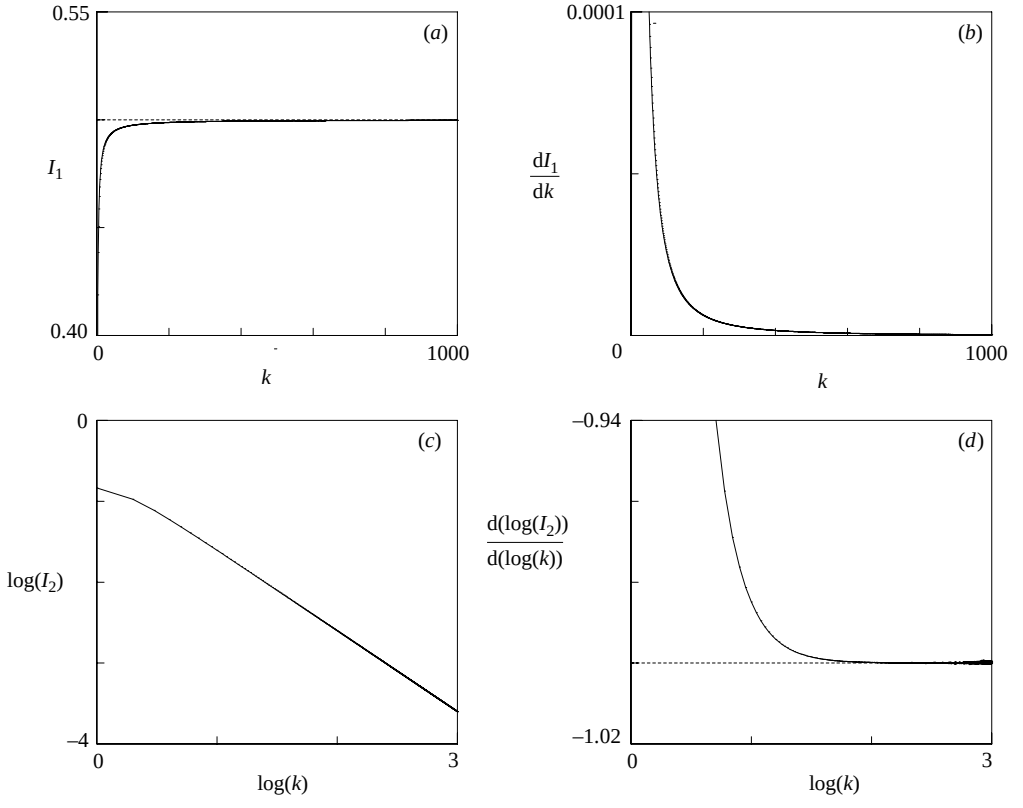

FIGURE 4. Behaviour of I_1, I_2 as $k \to \infty$. (*a*) I_1 *vs.* k. The dashed line indicates the limiting behaviour $I_1 \to 0.5$ as $k \to \infty$. (*b*) $\mathrm{d}I_1/\mathrm{d}k$ *vs.* k. (*c*) $\log(I_2)$ *vs.* $\log k$. (*d*) $\mathrm{d}(\log I_2)/\mathrm{d}(\log k)$ *vs.* $\log k$. The dashed line indicates the limiting behaviour $\mathrm{d}(\log I_2)/\mathrm{d}(\log k) \to -1$ as $k \to \infty$.

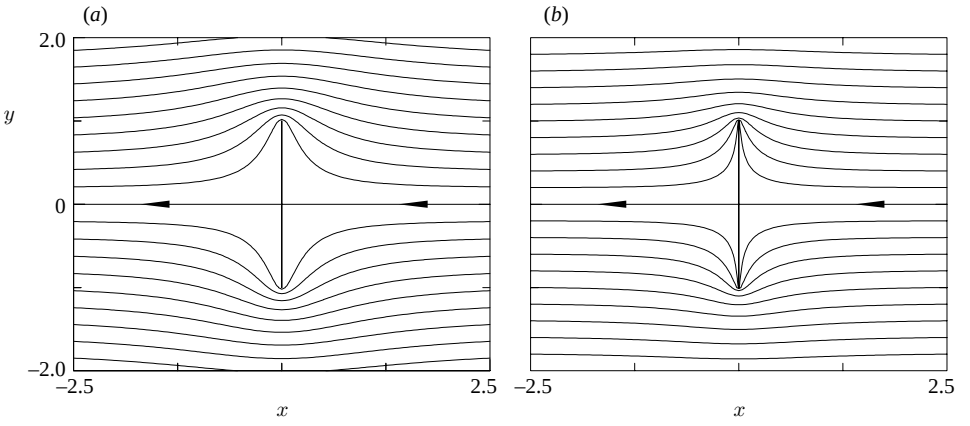

FIGURE 5. Potential flow past (*a*) a flat plate (*b*) a circular disk.

$\log k$. The curve appears to approach linear behaviour as $k \to \infty$. This is confirmed by figure 4(*d*), which plots the slope of the curve, and shows that it approaches -1 as $k \to \infty$. Thus,

$$I_1 \to \tfrac{1}{2}, \quad I_2 \sim \frac{1}{k} \text{ as } k \to \infty. \tag{4.16}$$

From this we can conclude that, just as in the vortex blob case, in the Euler-alpha case $w(k) \to 0$ as $k \to \infty$, but the decay rate is much slower. In the alpha model, the decay is algebraic, as

$$w_\alpha(k) \sim k^{-1/2}, \tag{4.17}$$

while in vortex blob method it is exponential,

$$w_\delta(k) \sim \sqrt{k}\mathrm{e}^{-k\delta/2}. \tag{4.18}$$

Thus, at small scales, the Euler-alpha model is less regularizing than the vortex blob one, consistent with our earlier remarks regarding the smoothing function h.

5. Model problem

5.1. *Initial conditions*

This section compares numerical solutions to the full regularized equations for an example of planar and axisymmetric vortex sheet flow. Following Krasny & Nitsche (2002), the initial conditions are given by potential flow past a flat plate in the planar case, and a flat disk in the axisymmetric case, as shown in figure 5. The flow is determined by Y, the plate half-span or disk radius, and U, the far-field velocity amplitude. The circulation between the tip of the plate at $y = Y$ and a point with coordinate y is known to be

$$\Gamma(y) = cU\sqrt{Y^2 - y^2}, \tag{5.1}$$

where $c_{2d} = 2$ and $c_{3d} = 4/\pi$. Subscripts $2d$ and $3d$ refer to the planar and the axisymmetric case, respectively.

The maximum circulation is $\Gamma_o = cUY$. The results are presented in non-dimensional form where distance is scaled by Y and time by Y^2/Γ_o. The vortex sheet position and

circulation are parameterized by

$$x(\alpha, 0) = 0, \quad y(\alpha, 0) = \cos\alpha, \quad \Gamma(\alpha) = \sin\alpha, \quad \alpha \in I, \tag{5.2}$$

where $I_{2d} = [-\pi/2, \pi/2]$ and $I_{3d} = [0, \pi/2]$, corresponding to $Y = 1$, $\Gamma_o = 1$ and $U_{2d} = 1/2$, $U_{3d} = \pi/4$. Both initial flows are symmetric about $y = 0$ and remain so for all times. Notice that the initial circulation distribution is singular at $y = 1$ and therefore it is necessary to regularize the flow to compute its evolution.

5.2. *Numerical method*

The regularized evolution equations are given by (4.1), where u, v are the planar or axisymmetric Euler-alpha or vortex blob velocities. The equations are solved by discretizing the sheet by a finite number of points in the upper half-plane with coordinates $(x_j(t), y_j(t))$, $j = 0, \ldots, N$, $y_j \geqslant 0$, corresponding to a discretization of the parameter $\alpha \in [0, \pi]$. In the planar case, the position of image particles with $y < 0$ is determined by symmetry. The integrals in (4.1) are approximated by the trapezoid rule on these points. This yields a system of ordinary differential equations for the point position

$$\frac{\mathrm{d}x_i}{\mathrm{d}t} = \sum_{j=0}^{N} u_{ij}\Delta\Gamma_j, \qquad \frac{\mathrm{d}y_i}{\mathrm{d}t} = \sum_{j=0}^{N} v_{ij}\Delta\Gamma_j, \tag{5.3}$$

where $u_{ij} = u(x_i, y_i; x_j, y_j)$, $v_{ij} = v(x_i, y_i; x_j, y_j)$, and $\Delta\Gamma_j$ are the trapezoid weights, that is solved using the fourth-order Runge–Kutta method. The sums in (5.3) are evaluated by direct summation. The numerical cost is halved because u_{ij} and u_{ji} share common factors.

The computational meshpoints are initially uniformly spaced in α, corresponding to increasing point density near the tip of the sheet at $y = 1$. The initial number of points is N_0. As in previous work (Krasny 1987), at later times, new points are inserted whenever the angle that two consecutive points make with the vortex centre is bigger than a given value π/N_c, or when the distance between two consecutive points is bigger than a given parameter ϵ, where N_c and ϵ are user-specified. The points are inserted using cubic polynomial interpolants. For each value of the parameters $\alpha, \delta > 0$ shown below, the parameters N_o, N_c, ϵ and the time step Δt are chosen so that the solution has converged and remains unchanged under further refinement. More details on the numerical evaluation of u_{ij}, v_{ij} in the planar and axisymmetric case and on the corresponding computational cost are given below.

5.3. *Planar case*

5.3.1. *Computational issues*

The modified Bessel function of the second kind, K_1, required for the planar Euler-alpha regularization is evaluated using the routine kzeone.f from the Netlib repository (2005, http://www.netlib.org). Evaluating these Bessel functions dominates the computational cost in the Euler-alpha simulations, which is significantly higher than in the vortex blob simulations. To illustrate, the results presented in the next subsection for $\alpha = \delta = 0.2$ up to time $t = 60$, use parameters $N_0 = 400$, $N_c = 30$, $\epsilon = 0.04$ and $\Delta t = 0.025$, and the final number of points at $t = 60$ was $N = 2762$ in the vortex blob case and $N = 4324$ in the Euler-alpha case. The computing time was 13.5 min in the vortex blob case, and 10.5 h in the Euler-alpha case, on a 3.2 GHz PC.

5.3.2. *Solution for $\alpha = \delta = 0.2$, up to $t = 60$*

Figure 6 plots the vortex sheet evolution for $\alpha = \delta = 0.2$ and all other parameters as listed above. The vortex blob results from Krasny & Nitsche (2002) are shown in

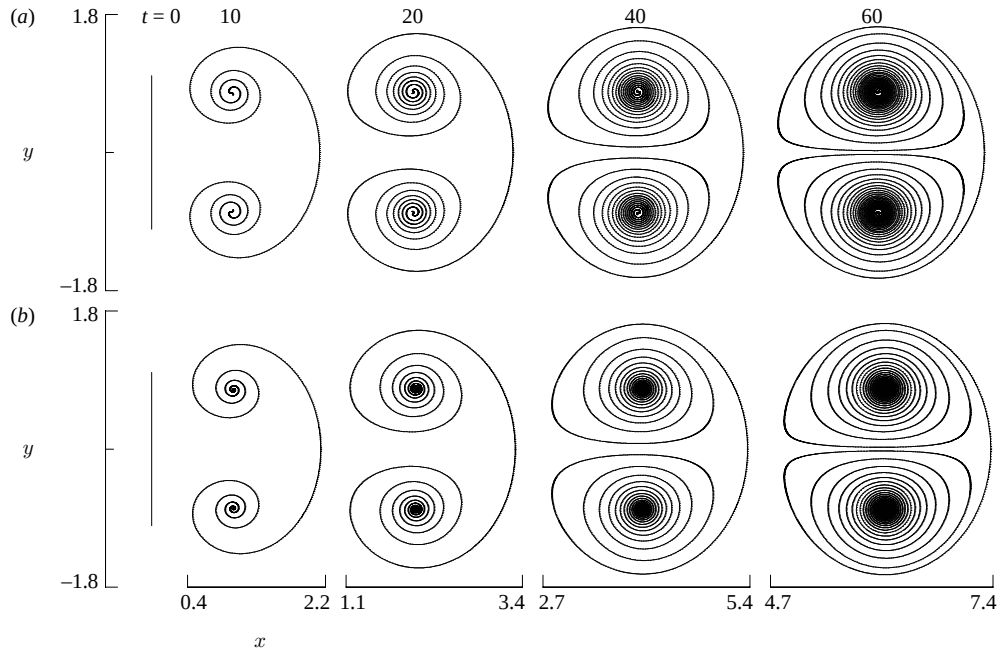

FIGURE 6. Planar vortex sheet roll-up at the indicated times, computed with $\alpha = \delta = 0.2$. (a) Vortex blob regularization. (b) Euler-alpha regularization.

figure 6(a), the new Euler-alpha results are shown in figure 6(b). The sheet is plotted in a reference frame fixed at infinity. In this frame, the initial condition corresponds to a plate which is impulsively moved to the right with velocity U, and immediately dissolved. The vortex sheet remaining in the flow moves under its self-induced velocity in the direction of the impulse as it rolls up at its edges into a spiral. The vorticity is concentrated at the spiral centre and the roll-up approximates a vortex pair.

The figure shows that, just as in the vortex blob case, the Euler-alpha model regularizes the motion sufficiently to compute vortex sheet roll-up. The large-scale features of the roll-up obtained with the two regularizations are similar. The translation velocity is only slightly faster in the Euler-alpha case. The shape of the outer vortex sheet turns also appears to be almost identical. However, some differences can be observed near the vortex centre. At small times ($t = 10, 20$), the roll-up in the alpha model is tighter near the spiral centre, and contains more spiral turns. The same is true at later times. Figure 7 plots a closeup of the solution at $t = 60$. It shows that at this time as well, while the outer turns are similar, the Euler-alpha roll-up contains more spiral turns near the vortex centre. The total number of turns is 23 in the vortex blob case, and 36 in the Euler-alpha case. As a result, the final number of points is also larger in the Euler-alpha case ($N = 4324$) than in the vortex blob case ($N = 2762$), contributing in part to the increased numerical cost. Finally, the Euler-alpha roll-up appears to be more regular than the vortex blob one. As shown in the simulations by Krasny & Nitsche (2002), core vorticity oscillations induce a chaotic resonance band in the vortex centre, the beginning of which is barely visible in figure 7(a). At the time $t = 60$ shown here, no irregularities are visible in the Euler-alpha case.

The differences observed near the spiral centre are caused by the differences in the corresponding smoothing kernels near the origin which were discussed earlier. Let (x_{core}, y_{core}) be the coordinates of the vorticity maximum. To gain more insight,

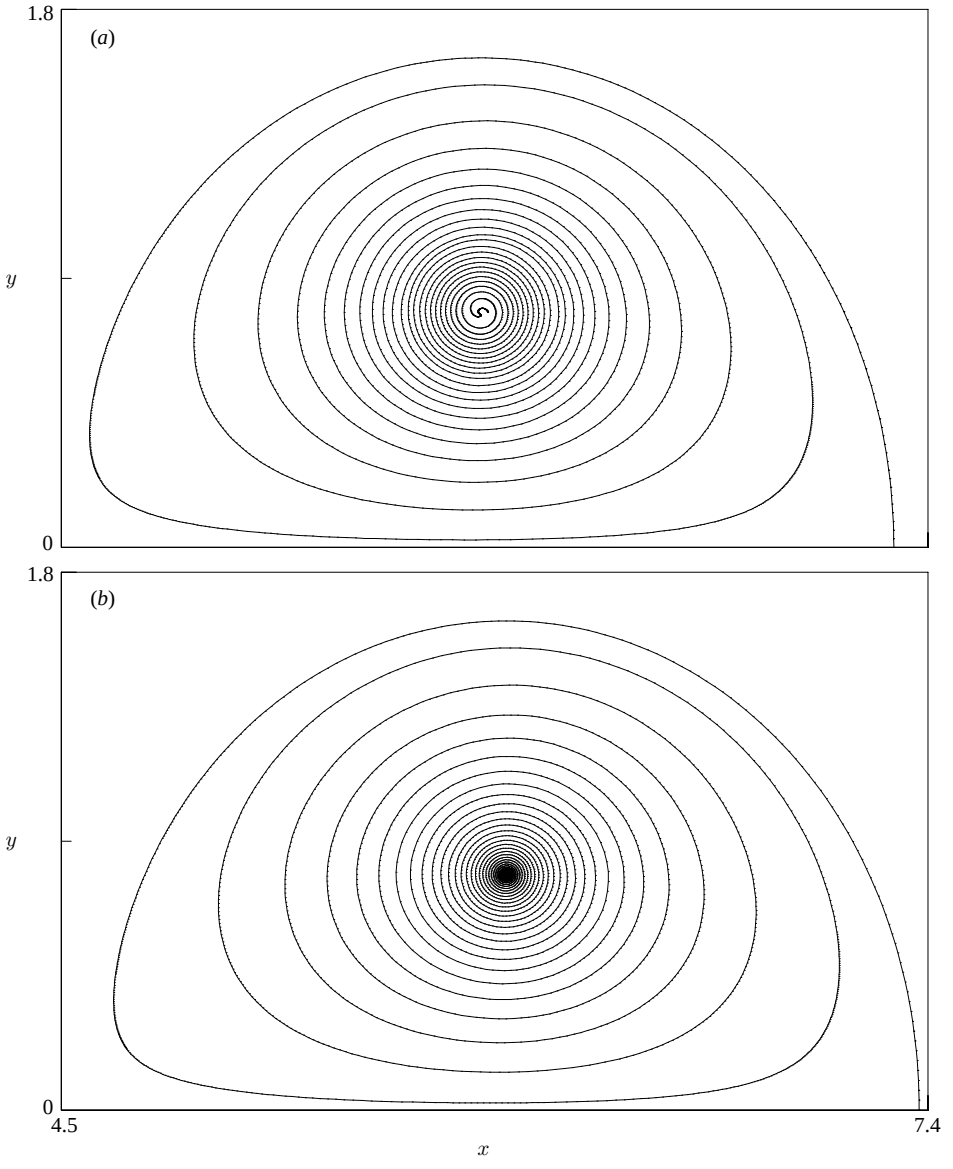

FIGURE 7. Closeup of the planar vortex sheet roll-up at $t = 60$, computed with $\alpha = \delta = 0.2$. (*a*) Vortex blob regularization, (*b*) Euler-alpha regularization.

figure 8 plots the regularized sheet's horizontal velocity (figure 8*a*) and vorticity (figure 8*b*) along a vertical line $x = x_{core}$ through the vorticity maximum. Figure 8(*b*) shows that the vorticity maximum is attained at approximately the same value of y_{core}, although the maximal value is larger in the Euler-alpha than in the blob case. Furthermore, while the vorticity profile is smooth in the blob case, it has a cusp at the maximum in the Euler-alpha case. To understand this, remember that in the Euler-alpha case the vorticity associated with a point vortex, given by (3.11), is unbounded, with a logarithmic singularity at the origin. Since the logarithm is integrable, the superposition of point vortices representing the vortex sheet has bounded vorticity. At its maximum, the vorticity has a cusp with unbounded spatial derivatives.

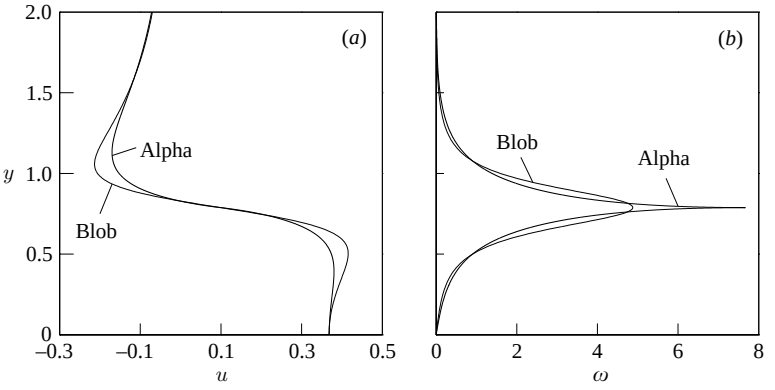

FIGURE 8. (*a*) Horizontal velocity and (*b*) scalar vorticity of the planar vortex sheet at $t = 60$ along a vertical line through the vorticity maximum, regularized by the vortex blob and the Euler-alpha model with $\alpha = \delta = 0.2$, as indicated.

At the vorticity maximum ($y = y_{core}$), the horizontal velocity shown in figure 8(*a*) is positive and is representative of the vortex translation velocity. The flow rotates about the vorticity maximum and therefore the velocities are larger for $y < y_{core}$ and smaller for $y > y_{core}$. The absolute velocities in a region surrounding the core are larger in the vortex blob case. As a result, the vortex blob vorticity (figure 8*b*) is slightly larger in a region surrounding the core, but not at the core.

5.3.3. *Dependence on* α, δ *at* $t = 20$

Figures 6–8 show that, while the large-scale spiral features obtained with $\alpha = \delta = 0.2$ agree well, there are differences in the vortex core. We may argue that it is not appropriate to compare equal values of α and δ, but that they should be chosen, for example, so that the maximum regularized velocities agree. To estimate the effect of variations in α and δ better, figures 9 and 10 summarize the results at a fixed time $t = 20$, for a range of values $\alpha, \delta \in [0.07, 0.5]$. Following Krasny (1986*b*), figure 9 plots the maximum and minimum y-coordinate y_{max} on each vortex sheet turn, as a function of α, δ. Points corresponding to the same vortex sheet turn, starting from outside, are connected by a curve. The vortex blob results are shown in figure 9(*a*), the Euler-alpha results in figure 9(*b*). The figure indicates the number of spiral turns for each value of the regularization parameter, and the change in that turn as the parameter varies. For example, for $\delta = 0.3$ there are 6 intersections corresponding to 3 vortex sheet turns in the vortex blob case, and 9 intersections corresponding to 4 $\frac{1}{2}$ vortex sheet turns in the Euler-alpha case. In each case, the spiral turn amplitudes slightly increase as the regularization parameter decreases. Based on the results in this figure, in both cases the values y_{max} corresponding to the same spiral turn appear to converge as $\delta \to 0$. The shape of the curves differs slightly, but the limiting values appear to be similar. In agreement with figures 6 and 7, for fixed value δ, the alpha model has more turns than the vortex blob model. Also, the innermost spiral turn shown has a larger radius in (*a*) than in (*b*), in agreement with figure 7.

Figure 10 plots the circulation parameter Γ_{int} at the points of maximum and minimum y-coordinate on each vortex sheet turn, connected by a curve. Again, these curves appear to converge as $\alpha, \delta \to 0$, and the limits appear to be similar. There are more curves in figure 10(*b*) than in figure 10(*a*), since there are more vortex sheet turns. A noticeable difference is that the circulation in the inner turns is much smaller

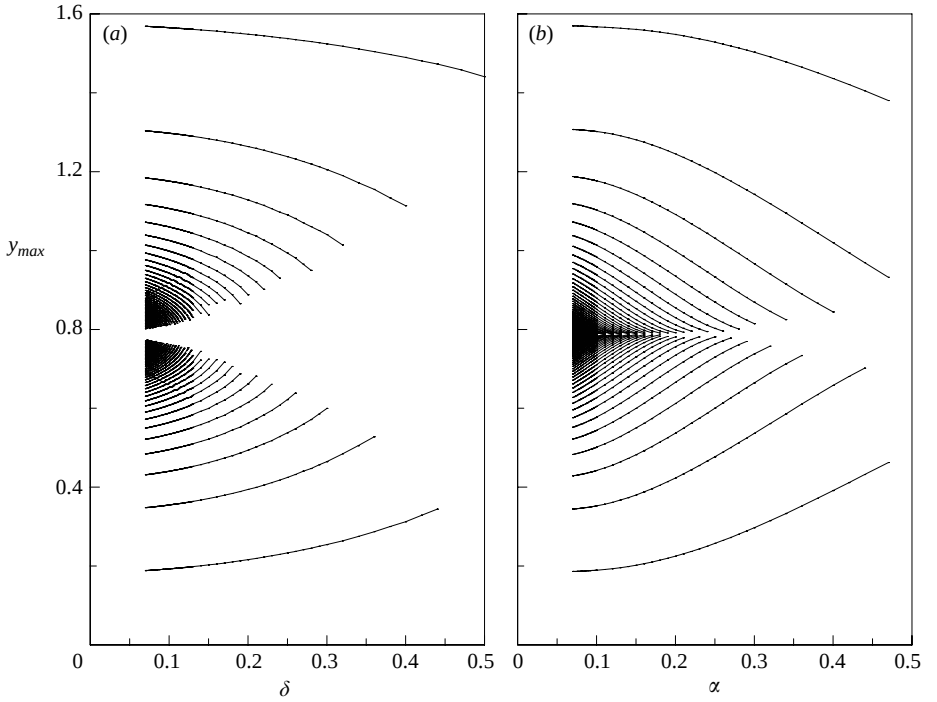

FIGURE 9. Maximum and minimum vertical/radial coordinate y on each turn of the planar vortex sheet at $t = 20$, for a range of values $0.07 \leqslant \alpha, \delta \leqslant 0.5$, using ($a$) the vortex blob regularization, and (b) the Euler-alpha regularization.

in the Euler-alpha case than in the vortex blob case. For example, for $\alpha = \delta = 0.1$, the innermost turn contains approximately 30 % of the total circulation in the vortex blob case, but only 2 % in the Euler-alpha case.

From the results shown in this section, we conclude that, similar to the vortex blob model, the Euler-alpha model sufficiently regularizes vortex sheet motion to compute vortex sheet roll-up. However, significant differences are visible near the spiral centre, independent of specific values of α, δ. The Euler-alpha roll-up contains more spiral turns in the core and the innermost turn is smaller and has much smaller circulation than in vortex blob case. While it is expected that as $\alpha, \delta \to 0$ the circulation and radius of the innermost spiral turn vanish, this limit appears to be approached faster in the Euler-alpha than in the vortex blob case. This reflects the fact that the Euler-alpha kernel is closer to the unregularized case than the vortex blob kernel.

The next section presents a brief comparison in the axisymmetric case.

5.4. *Axisymmetric vortex sheet motion*

5.4.1. *Computational issues*

It is more costly to compute the Euler-alpha velocities, given by (3.19), than to compute the vortex blob velocities, given by (3.21). The vortex blob integrals in (3.21) can be expressed in terms of elliptic functions and evaluated fast and accurately using available algorithms. We use the method of arithmetic–geometric means as proposed by Bulirsch (1965). In the alpha model, the integrals in (3.19) cannot be reduced to known functions and must be approximated via numerical integration. Although the integrands are periodic functions of θ, the behaviour near $\theta = 0$ is almost singular if (x, y) is near (x_o, y_o), and accurate integration becomes extremely expensive.

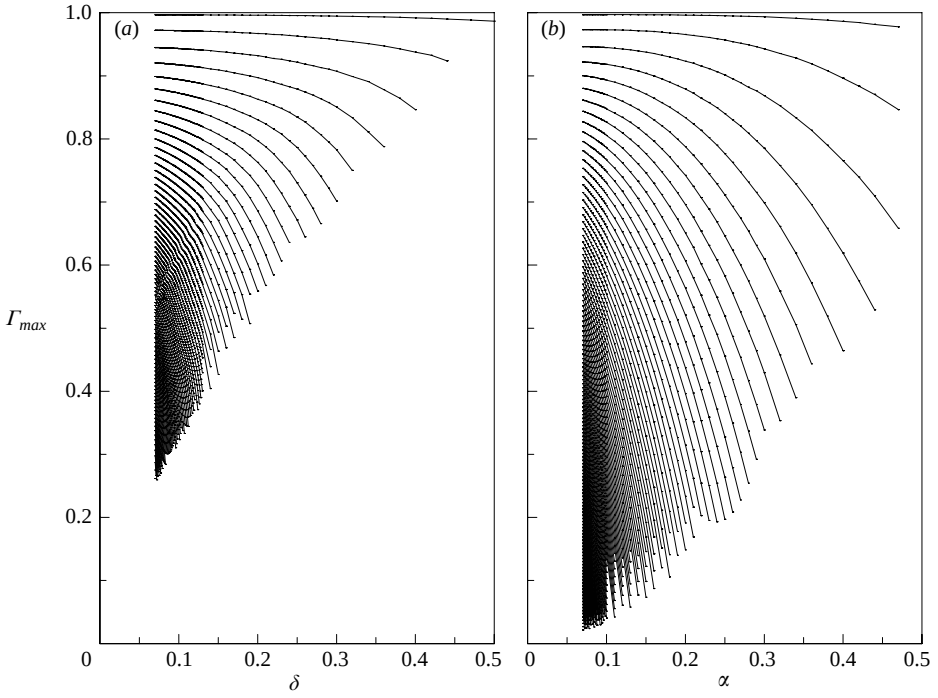

FIGURE 10. Circulation Γ at the points of maximum and minimum coordinate y on each turn of the planar vortex sheet at $t = 20$, for a range of values $0.07 \leqslant \alpha, \delta \leqslant 0.5$, using (*a*) vortex blob regularization, (*b*) the Euler-alpha regularization.

Here, the computational expense is reduced by first rewriting the integrals (3.19*a*, *b*) in terms of functions f_1, f_2 as follows,

$$u_\alpha(x, y; x_o, y_o) = \frac{\Gamma_o y_o}{\pi}\,[2yf_2 - (y - y_o)f_1], \tag{5.4a}$$

$$v_\alpha(x, y; x_o, y_o) = \frac{\Gamma_o (x - x_o) y_o}{\pi}\,[f_1 - 2f_2], \tag{5.4b}$$

where

$$f_1 = \int_0^{\pi/2} g(r)\,\mathrm{d}\phi, \quad f_2 = \int_0^{\pi/2} g(r)\sin^2\phi\,\mathrm{d}\phi, \tag{5.5a}$$

$$g(r) = \frac{1 - \mathrm{e}^{-r/\alpha}(1 + r/\alpha)}{r^3}, \tag{5.5b}$$

$$r(\phi) = \sqrt{(x - x_o)^2 + (y - y_o)^2 + 4yy_o\sin^2\phi}. \tag{5.5c}$$

Then, we use the fact that

$$g(r) \sim \frac{1}{2\alpha^2 r}, \tag{5.6}$$

where $f \sim g$ denotes that $f - g$ is smoother than f, to approximate f_1, f_2 by elliptic integrals, as follows

$$f_1 \sim \tilde{f}_1 = \frac{1}{\sqrt{a^2 + b^2}}F(c), \quad f_2 \sim \tilde{f}_2 = \frac{-a^2}{b^2\sqrt{a^2 + b^2}}F(c) + \frac{\sqrt{a^2 + b^2}}{b^2}E(c), \tag{5.7}$$

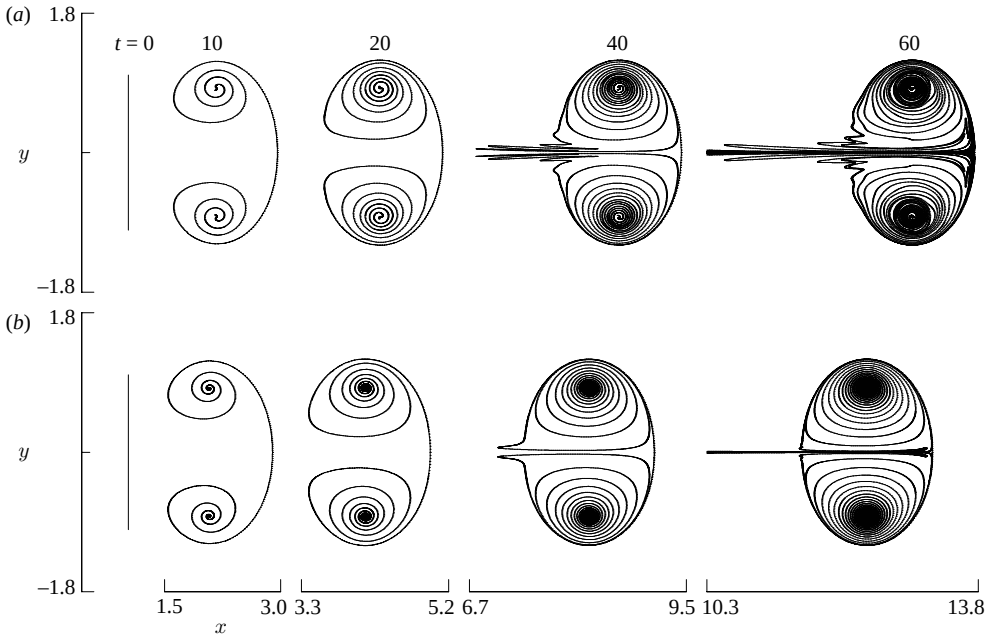

FIGURE 11. Axisymmetric vortex sheet at the indicated times, computed with (*a*) vortex blob regularization (*b*) Euler-alpha regularization.

where $a^2 = (x - x_o)^2 + (y - y_o)^2$, $b^2 = 4yy_o$, $c^2 = b^2/(a^2 + b^2)$, and E and F are the complete elliptic integrals of the first and second kind. Since $f_k - \tilde{f}_k$ is smoother than f_k, it is integrated accurately using fewer points, and $\tilde{f}_k$ is evaluated fast using the method of arithmetic–geometric means. The contribution $u_{ij}\Delta\Gamma_j$ is computed to within an error of less than 10^{-12}, using the trapezoid rule. The integration error is estimated by the difference between two approximations using m and $2m$ points. If the difference is larger than the desired error, the number of points is doubled and the process repeated. The number of points required to evaluate u_{ij} ranges between 16 and 4096, depending on how small the corresponding value of a^2 is. This method guarantees overall accuracy at reasonable cost. Nonetheless, the computational cost is high. The simulation presented below for $\delta = \alpha = 0.2$ up to $t = 60$ used parameters $N_c = 25$, $\Delta t = 0.025$, $N_o = 400$, and the final number of points at $t = 60$ are $N = 6392$ and $N = 3888$ in the vortex blob and Euler-alpha case, respectively. These runs took took about 4 h in the vortex blob case, and 110 h in the Euler-alpha case.

As an alternative, we considered precomputing f_1, f_2 on a mesh and interpolating these values for each required pair (a, b), but found that variations near $a = 0$ are too large for this approach to be practical while retaining accuracy.

5.4.2. *Solution for $\alpha = \delta = 0.2$, up to $t = 60$*

Figure 11 plots the axisymmetric vortex sheet evolution at the times indicated, using $\alpha = \delta = 0.2$ and all other parameters as listed above. The vortex blob results from Krasny & Nitsche (2002) are shown in figure 11(*a*), the new Euler-alpha results in figure 11(*b*). Under both regularizations, the sheet rolls up into an elliptically shaped vortex ring and translates in the direction of the initial impulse. The sheet travels slightly faster in the vortex blob case. As in the planar case, the shape of the outer spiral turns is similar, while the inner spiral roll-up is tighter, more regular and

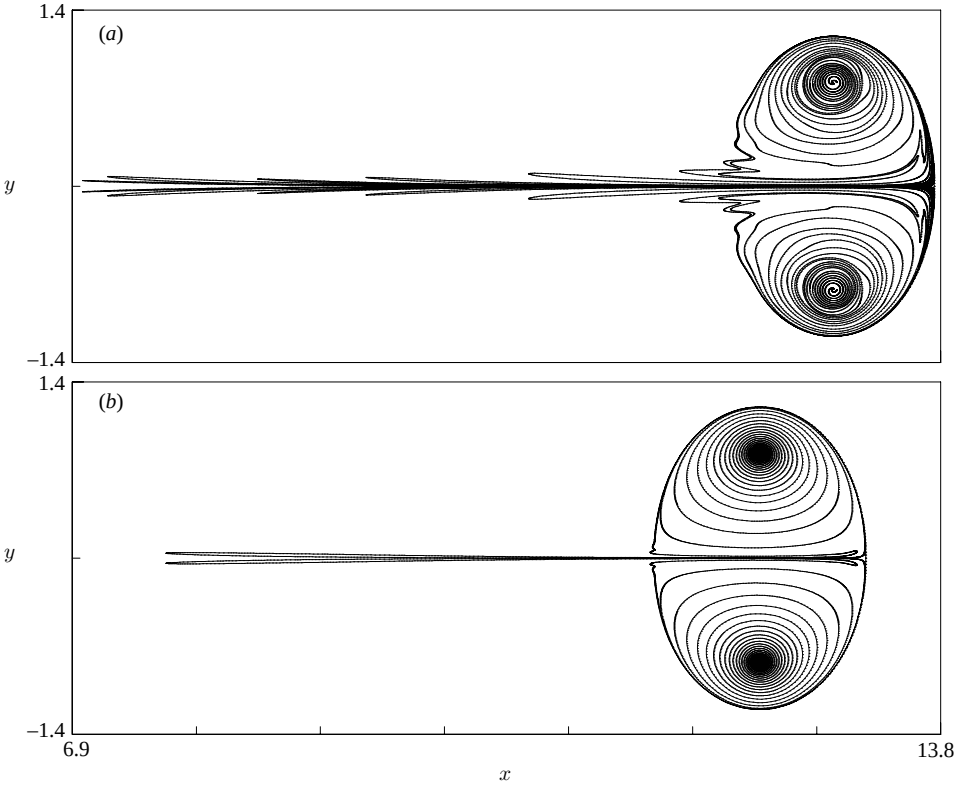

FIGURE 12. Axisymmetric sheet at $t = 60$, computed with (a) vortex blob regularization (b) Euler-alpha regularization.

with more spiral turns in the Euler-alpha case. With both regularizations, the ring develops a tail of particles that leave the bubble of fluid moving with the ring and are left behind. As discussed by Krasny & Nitsche (2002), this tail corresponds to a heteroclinic tangle that develops owing to oscillations in the core vorticity. Figure 11 plots only part of the tail at $t = 60$. A closeup of the full solution is shown in figure 12.

The closeup displays the similarities and differences between the two cases more clearly. While the elliptical rollup and the shape of the outer spiral turns are similar, the particle motion is more regular in the Euler-alpha case, both in the tail and in the core. The Euler-alpha tail is shorter, reflecting the fact that the particle shedding began slightly later in this case. Furthermore, the Euler-alpha tail has fewer lobes. A close inspection of figure 12 shows that in the vortex blob case, the tail has six well-established lobes and three nascent ones, while in the Euler-alpha case there is one well-established lobe and two nascent ones. As explained by Krasny & Nitsche (2002), oscillations in the core vorticity are responsible for both irregular particle motion in the core owing to a resonance band and the formation of a tail owing to a heteroclinic tangle. Because a tail is present in both cases, we can deduce the presence of core vorticity oscillations. The fact that the number of lobes in the tail differs reflects possible differences in the oscillation frequency, which may explain differences in the regularity of the roll-up. A detailed study of the effect of the regularization on the irregular behaviour observed in Krasny & Nitsche (2002) is outside the scope of this paper and will be presented elsewhere.

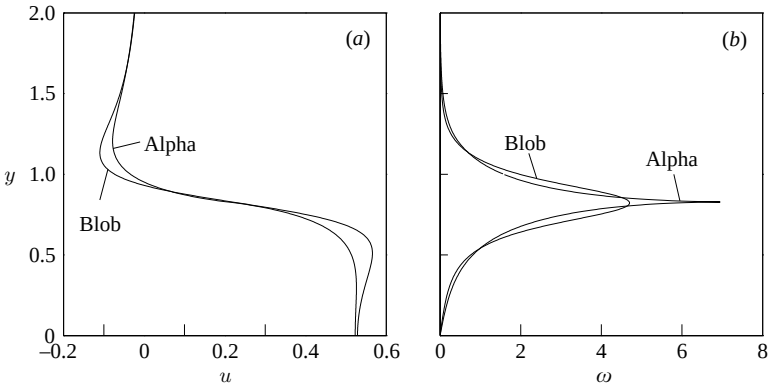

FIGURE 13. (*a*) Radial velocity and (*b*) azimuthal vorticity of the axisymmetric vortex sheet at $t = 60$ along a vertical line through the vorticity maximum, regularized by the vortex blob and the Euler-alpha model with $\alpha = \delta = 0.2$, as indicated.

To conclude this section, figure 13 compares the regularized horizontal velocity and the regularized vorticity along a vertical line through the vortex core. As in the planar case, the vortex blob velocity is slightly larger in a region surrounding the core, with corresponding larger vorticity values, but at the core, the Euler-alpha vorticity is larger. As in the planar case, the Euler-alpha vorticity has a cusp at the vorticity maximum while the vortex blob vorticity is smooth. The cusp in the Euler-alpha case is the result of integrating the logarithmic singularity in the vorticity associated with a circular vortex filament, which is integrable.

6. Summary

The Euler-alpha and the vortex blob method are two regularizations of inviscid fluid flow that share a common framework with two differing kernel functions. In this paper, we first present the parallels between the two regularizations within the framework first developed in the Euler-alpha case by Holm *et al.* (1998*a*, *b*). We then apply the regularizations to vortex filament and vortex sheet motion and compare the results.

While the vortex blob kernel is bounded and smooth, the Euler-alpha kernel is unbounded at the origin and thereby closer to the unregularized case. Our numerical comparison addresses the resulting question of how the difference in the kernel affects the regularized flow evolution, in the case of singular initial data such as filaments and sheets. The main results are as follows.

Vortex filament regularization. (*i*) The vorticity corresponding to a regularized planar point vortex and a regularized axisymmetric vortex filament is unbounded in the Euler-alpha case, while bounded in the blob case. (*ii*) An analytic approximation for the self-induced velocity of a regularized axisymmetric filament is given. For equal regularization parameter, the self-induced velocity is higher in the vortex blob case than in the Euler-alpha case.

Vortex sheet stability. Linear stability analysis of a flat vortex sheet shows that the Euler-alpha regularization damps the high wavenumber growth, just as the vortex blob regularization, although at a slower rate. The decay is algebraic instead of exponential.

Vortex sheet roll-up. The Euler-alpha model, just as the vortex blob model, sufficiently regularizes planar and axisymmetric vortex sheet motion to compute

vortex sheet roll-up. The main similarities and differences are as follows. (*i*) The large-scale features of the roll-up, such as the shape of the outer vortex sheet turns, the translation velocity, and the presence of a tail in the axisymmetric case, are in good agreement. (*ii*) The Euler-alpha and the vortex blob roll-up differ near the vortex core. The core vorticity is smooth in the vortex blob case, and bounded but singular (cusp) in the Euler-alpha case. The Euler-alpha case has significantly more vortex sheet turns containing the core vorticity, and the roll-up is more regular. (*iii*) Differences in the number of lobes of the axisymmetric tail suggest that the increased regularity is due to differences in core vorticity oscillation frequency and magnitude. This item, as well as details of the behaviour as the regularization parameter vanishes, remain to be explored. (*iv*) The Euler-alpha simulations are computationally more costly than the vortex blob ones. The planar case requires the evaluation of Bessel functions; the axisymmetric case requires numerical integration in the azimuthal direction.

D. D. H. is grateful for partial support by US DOE, under contract W-7405-ENG-36 for Los Alamos National Laboratory, and Office of Science ASCAR/AMS/MICS. M. N. gratefully acknowledges the support of the National Science Foundation through grant DMS-0308061. V. P. is grateful for support by US DOE through grant DE-FG02-04ER-46119 and the Petroleum Research Fund through grant 40218-AC9.

Appendix A. Conservation laws for Euler-alpha and vortex blob models

Solutions of the vortex blob regularization and the Euler-alpha model both fit into the same Hamiltonian framework, albeit with different smoothing operators and thus different Hamiltonian functions. The motion equations are obtained using the Lie–Poisson bracket,

$$\{F, H\} = \int \boldsymbol{q} \cdot \operatorname{curl} \frac{\delta F}{\delta \boldsymbol{q}} \times \operatorname{curl} \frac{\delta H}{\delta \boldsymbol{q}} \, \mathrm{d}^3x.$$

This Lie–Poisson bracket was first introduced for the Euler equations in Kuznetsov & Mikhailov (1980) and was discussed further in that context in Marsden & Weinstein (1983). The Lie–Poisson bracket is defined on the dual with respect to the L^2 pairing $\langle \cdot, \cdot \rangle$ of the Lie algebra of divergence-less vector fields. Namely,

$$\{F, H\} = \left\langle \boldsymbol{q}, \left[\frac{\delta F}{\delta \boldsymbol{q}}, \frac{\delta H}{\delta \boldsymbol{q}} \right] \right\rangle.$$

Being a linear functional of a Lie–algebra bracket, the Lie–Poisson bracket is skew symmetric and satisfies the Jacobi identity. Thus, it is a *bona fide* Poisson bracket.

The Hamiltonian takes the same form,

$$H = \tfrac{1}{2} \int \boldsymbol{u} \cdot \boldsymbol{v} \, \mathrm{d}^3x = \tfrac{1}{2} \int \boldsymbol{\psi} \cdot \boldsymbol{q} \, \mathrm{d}^3x.$$

In either case, the Lie–Poisson motion equation for circulation vorticity takes the Euler form,

$$\frac{\partial}{\partial t} \boldsymbol{q} = \{\boldsymbol{q}, H\} = -\operatorname{curl}(\boldsymbol{q} \times \operatorname{curl} \boldsymbol{\psi}) = \operatorname{curl}(\boldsymbol{u} \times \boldsymbol{q}) = -\boldsymbol{u} \cdot \nabla \boldsymbol{q} + \boldsymbol{q} \cdot \nabla \boldsymbol{u},$$

and thus depends on the particular regularization h chosen, through the relation $\boldsymbol{u} = h * \boldsymbol{v} = \operatorname{curl} \boldsymbol{\psi}$ and their different circulation vorticities $\boldsymbol{q} = \operatorname{curl} \boldsymbol{v}$. As discussed

in § 3, the regularizing function is $h = h_\alpha$ in the Euler-alpha case, and $h = h_\delta$ in the vortex blob case. Both of these are invariant under translations and rotations. Consequently, their Hamiltonians inherit these symmetries. Hence, both models conserve the quantities that Poisson-generate these transformations. Namely, they conserve the linear momentum

$$L = \tfrac{1}{2}\int \boldsymbol{q} \times \boldsymbol{x}\, \mathrm{d}^3x = \int \boldsymbol{v}\, \mathrm{d}^3x,$$

which Poisson-generates spatial translations, and the angular momentum

$$I = -\tfrac{1}{2}\int |\boldsymbol{x}|^2 \boldsymbol{q}\, \mathrm{d}^3x = \int \boldsymbol{v} \times \boldsymbol{x}\, \mathrm{d}^3x,$$

which Poisson-generates spatial rotations. In addition, the Lie–Poisson bracket has the Casimir function

$$C = \int \boldsymbol{v} \cdot \boldsymbol{q}\, \mathrm{d}^3x,$$

which satisfies $\{C\,,\ H\} = 0$ for every Hamiltonian H, since its variational derivative satisfies $\mathrm{curl}(\delta C/\delta \boldsymbol{q}) = 2\boldsymbol{q}$. In summary, the vortex blob regularization and the Euler-alpha model both share the same Hamiltonian properties and conservation laws as the Euler equations.

Appendix B. Self-induced velocity of a circular vortex filament, regularized by Euler-alpha

The self-induced velocity of a regularized circular filament of radius R is obtained from (3.19) by setting $x = x_0$ and $y = y_0 = R$. In this case,

$$\rho = \sqrt{2}R\sqrt{1-\cos\theta} = 2R\sin\tfrac{1}{2}\theta = 2R\sin\phi, \quad \phi = \tfrac{1}{2}\theta, \quad \theta \in [0, 2\pi], \tag{B 1}$$

which is equal to zero only when $\theta = 0, \pi$. It is therefore easy to see that $v_\alpha(x_0, R; x_0, R) = 0$. The filament's translation velocity is

$$\begin{aligned} u_\alpha(x_0, R; x_0, R) &= \frac{\Gamma}{4\pi}\int_0^{2\pi} \frac{1 - \mathrm{e}^{-\rho/\alpha}(1+\rho/\alpha)}{\rho^3} R^2(1-\cos\theta)\,\mathrm{d}\theta \\ &= \frac{\Gamma}{4\pi}\int_0^{2\pi} \frac{1 - \mathrm{e}^{-\rho/\alpha}(1+\rho/\alpha)}{\rho^3} \frac{\rho^2}{2}\,\mathrm{d}\theta \\ &= \frac{\Gamma}{4\pi}\int_0^{\pi} \frac{1 - \mathrm{e}^{-\rho/\alpha}(1+\rho/\alpha)}{\rho}\,\mathrm{d}\phi \\ &= \frac{\Gamma}{2\pi}\int_0^{\pi/2} \frac{1 - \mathrm{e}^{-\rho/\alpha}(1+\rho/\alpha)}{\rho}\,\mathrm{d}\phi \\ &= \frac{\Gamma}{2\pi}\int_0^{2R} \frac{1 - \mathrm{e}^{-\rho/\alpha}(1+\rho/\alpha)}{\rho} \frac{\mathrm{d}r}{\sqrt{4R^2-\rho^2}} = \frac{\Gamma}{2\pi} I, \end{aligned} \tag{B 2}$$

where we used the fact that

$$\int_0^{\pi} f(\sin\phi)\,\mathrm{d}\phi = 2\int_0^{\pi/2} f(\sin\phi)\,\mathrm{d}\phi.$$

The integral I can be estimated by writing $I = I_0 + (I - I_0)$, where

$$I_0 = \frac{1}{2R}\int_0^{2R} \frac{1-\mathrm{e}^{-\rho/\alpha}(1+\rho/\alpha)}{\rho}\,\mathrm{d}\rho = \frac{1}{2R}\int_0^{2R/\alpha} \frac{1-\mathrm{e}^{-x}(1+x)}{x}\,\mathrm{d}x$$
$$= \frac{1}{2R}\left[\int_0^{2R/\alpha} \frac{1-\mathrm{e}^{-x}}{x}\,\mathrm{d}x - \int_0^{2R/\alpha} \mathrm{e}^{-x}\,\mathrm{d}x\right] = \frac{1}{2R}\left[Ein(2R/\alpha) + \left(\mathrm{e}^{-2R/\alpha}-1\right)\right]. \quad (B\,3)$$

The exponential integral function satisfies

$$Ein(z) = \int_0^z \frac{1-\mathrm{e}^{-x}}{x}\,\mathrm{d}x = \int_0^{10} \frac{1-\mathrm{e}^{-x}}{x}\,\mathrm{d}x + \int_{10}^z \frac{1}{x}\,\mathrm{d}x - \int_{10}^z \frac{\mathrm{e}^{-x}}{x}\,\mathrm{d}x$$
$$= 2.879805 + \ln z - \ln 10 + error \;= \ln z + 0.577220 + error, \quad (B\,4)$$

where $z \geqslant 10$ and $|error| \leqslant \mathrm{e}^{-10}/10 < 0.5\times 10^{-5}$. The remaining difference $I - I_0$ can be evaluated by separating it into two integrals, of which the first can be evaluated exactly (using a trigonometric substitution) and the second can be approximated using Taylor series expansions:

$$I - I_0 = \int_0^{2R} \frac{1-\mathrm{e}^{-r/\alpha}(1+r/\alpha)}{r}\left[\frac{1}{\sqrt{4R^2-r^2}} - \frac{1}{2R}\right]\mathrm{d}r$$
$$= \frac{1}{2R}\int_0^{2R/\alpha} \frac{1-\mathrm{e}^{-x}(1+x)}{x}\left[\frac{1}{\sqrt{1-\alpha^2x^2/4R^2}} - 1\right]\mathrm{d}x$$
$$= \frac{1}{2R}\left\{\int_0^{2R/\alpha} \frac{1}{x}\left[\frac{1}{\sqrt{1-\alpha^2x^2/4R^2}} - 1\right]\mathrm{d}x\right.$$
$$\left. - \int_0^{2R/\alpha} \frac{\mathrm{e}^{-x}(1+x)}{x}\left[\frac{1}{\sqrt{1-\alpha^2x^2/4R^2}} - 1\right]\mathrm{d}x\right\}$$
$$= \frac{1}{2R}\left\{\int_0^1 \frac{1}{u}\left[\frac{1}{\sqrt{1-u^2}} - 1\right]\mathrm{d}u - \int_0^{2R/\alpha} \frac{\alpha^2}{8R^2}x(1+x)\,\mathrm{e}^{-x}\right.$$
$$\left. + O\left(\frac{\alpha^4}{R^4}\,\mathrm{e}^{-x}(1+x)x^3\right)\mathrm{d}x\right\}$$
$$= \frac{1}{2R}\left[\ln 2 - \frac{3\alpha^2}{8R^2} + O\left(\frac{\alpha^4}{R^4}\right)\right], \quad (B\,5)$$

where we used $\int_0^z x^m \mathrm{e}^{-x}\,\mathrm{d}x = m! + O(\mathrm{e}^{-z})$. The result is that the self-induced velocity is

$$u(x_0, R) = \frac{\Gamma}{4\pi R}\left[Ein\left(\frac{2R}{\alpha}\right) - 1 + \ln(2) - \frac{3\alpha^2}{8R^2} + O\left(\frac{\alpha^4}{R^4}\right)\right]$$
$$\approx \frac{\Gamma}{4\pi R}\left[\ln\left(\frac{R}{\alpha}\right) - 1 + 2\ln(2) + 0.577220 - \frac{3\alpha^2}{8R^2} + error + O\left(\frac{\alpha^4}{R^4}\right)\right], \quad (B\,6)$$

where $error < 0.5\times 10^{-5}$, assuming that $2R/\alpha > 10$. This result was confirmed numerically.

REFERENCES

Anderson, C. 1985 A vortex method for flows with slight density variations. *J. Comput. Phys.* **61**, 417–444.

Baker, G. R. & Pham, L. D. 2005 A comparison of blob methods for vortex sheet roll-up. *J. Fluid Mech.* **547**, 297–316.

Baker, G. R. & Shelley, M. J. 1990 On the connection between thin vortex layers and vortex sheets. *J. Fluid Mech.* **215**, 161–194.

Beale, J. T. & Majda, A. 1985 High order accurate vortex methods with explicit velocity kernels. *J. Comput. Phys.* **58**, 188–223.

Bulirsch, R. 1965 Numerical calculation of elliptic integrals and elliptic functions. *Numer. Maths* **7**, 78–90.

Caflisch, R. E., Ercolani, N., Hou, T. & Y. Landis, Y. 1993 Multi-valued solutions and branch point singularities for nonlinear hyperbolic or elliptic systems. *Commun. Pure Appl. Maths* **46**, 453–499.

Caflisch, R. E., Hou, T. Y. & Lowengrub, J. 1999 Almost optimal convergence of the point vortex method for vortex sheets using numerical filtering. *Math. Comput.* **68**, 1465–1496.

Camassa, R. & Holm, D. D. 1993 An integrable shallow-water equation with peaked solitons. *Phys. Rev. Lett.* **71**, 1661–1664.

Chen, S., Foias, C., Holm, D. D., Olson, E., Titi, E. S. & Wynne, S. 1999 The Camassa–Holm equations as a closure model for turbulent channel and pipe flow. *Phys. Rev. Lett.* **81**, 5338–5341.

Chorin, A. J. & Bernard, P. S. 1973 Discretization of a vortex sheet, with an example of roll-up. *J. Comput. Phys.* **13**, 423–429.

Cottet, G.-H. & Koumoutsakos, P. D. 2000 *Vortex Methods: Theory and Practice*. Cambridge University Press.

Cowley, S. J., Baker, G. & Tanveer, S. 1999 On the formation of Moore curvature singularities in vortex sheets. *J. Fluid Mech.* **378**, 233–267.

Foias, C., Holm, D. D. & Titi, E. S. 2001 The Navier–Stokes-alpha model of fluid turbulence. *Physica* D **152–153**, 505–519.

Holm, D. D. 2003 Rasetti–Regge Dirac bracket formulation of Lagrangian dynamics of vortex filaments. *Maths Comput. Simulation* **62**, 53–63.

Holm, D. D., Marsden, J. E. & Ratiu, T. S. 1998*a* Euler–Poincaré models of ideal fluids with nonlinear dispersion. *Phys. Rev. Lett.* **80**, 4173–4176.

Holm, D. D., Marsden, J. E. & Ratiu, T. S. 1998*b* The Euler–Poincaré equations and semidirect products with applications to continuum theories. *Adv. Maths* **137**, 1–81.

Hou, T., Lowengrub, J. & Shelley, M. 1997 The long time motion of vortex sheets with surface tension. *Phys. Fluids* **9**, 1933–1954.

Krasny, R. 1986*a* A study of singularity formation in a vortex sheet by the point-vortex approximation. *J. Fluid Mech.* **167**, 65–93.

Krasny, R. 1986*b* Desingularization of periodic vortex sheet roll-up. *J. Comput. Phys.* **65**, 292–313.

Krasny, R. 1987 Computation of vortex sheet roll-up in the Trefftz plane. *J. Fluid Mech.* **184**, 123–155.

Krasny, R. & Nitsche, M. 2002 The onset of chaos in vortex sheet flow. *J. Fluid Mech.* **454**, 47–69.

Kuznetsov, E. Z. & Mikhailov, A. V. 1990 On the topological meaning of canonical Clebsch variables. *Phys. Lett.* A **77**, 37–38.

Lamb, H. 1932 *Hydrodynamics*. Cambridge University Press.

Leonard, A. 1985 Computing three-dimensional incompressible flows with vortex elements. *Annu. Rev. Fluid Mech.* **17**, 523–559.

Majda, A. J. & Bertozzi, A. L. 2002 *Vorticity and Incompressible Flow*. Cambridge University Press.

Marsden, J. E. & Weinstein, A. 1983 Coadjoint orbits, vortices and Clebsch variables for incompressible fluids. *Physica* D **7**, 305–323.

Meiburg, E. 1995 Three-dimensional vortex dynamics simulations. In *Fluid Vortices* (ed. S. I. Green), pp. 651–685. Kluwer.

Meiron, D. I., Baker, G. R. & Orszag, S. A. 1982 Analytical structure of vortex sheet dynamics. Part 1. Kelvin–Helmholtz instability. *J. Fluid Mech.* **114**, 283–298.

Moore, D. W. 1979 The spontaneous appearance of a singularity in the shape of an evolving vortex sheet. *Proc. R. Soc. Lond.* A **365**, 105–119.

Nitsche, M. & Krasny, R. 1994 A numerical study of vortex ring formation at the edge of a circular tube. *J. Fluid Mech.* **276**, 139–161.

Puckett, E. G. 1993 Vortex methods: an introduction and survey of selected research topics. In *Incompressible Fluid Dynamics – Trends and Advances* (ed. R. A. Nicolaides & M. D. Gunzburger), pp. 335–407. Cambridge University Press.

Rosenhead, L. 1930 The spread of vorticity in the wake behind a cylinder. *Proc. R. Soc. Lond.* A **127**, 590–612.

Oliver, M. & Shkoller, S. 2001 The vortex blob method as a second-grade non-Newtonian fluid. *Commun. Partial Diffl Equat.* **26**, 295–314.

Saffman, P. G. 1992 *Vortex Dynamics.* Cambridge University Press.

Shelley, M. 1992 A study of singularity formation in vortex sheet motion by a spectrally accurate vortex method. *J. Fluid Mech.* **244**, 493–526.

Shkoller, S. 2000 Analysis on groups of diffeomorphisms of manifolds with boundary and the averaged motion of a fluid. *J. Diffl Geom.* **55**, 145–191.

Tryggvason, G., Dahm, W. J. A. & Sbeih, K. 1991 Fine structure of vortex sheet roll-up by viscous and inviscid simulation. *Trans. ASME* I: *J. Fluids Engng* **113**, 31–36.